1,3,7-triazapyrene-based ortho-carborane fluorophores : convenient synthesis, theoretical studies, and aggregation-induced emission properties

1,3,7-Triazapyrene-based *ortho*-Carborane Fluorophores: Convenient Synthesis, Theoretical Studies, and Aggregation-Induced Emission Properties

Lidia A. Smyshliaeva,[1,2] Mikhail V. Varaksin,[1,2]* Ekaterina I. Fomina,[1] Margarita V. Medvedeva,[1] Tatiana S. Svalova,[1] Alisa N. Kozitsina,[1] Oleg P. Demidov,[3] Ivan V. Borovlev,[3] Carl Mensch,[4] Pieter Mampuys,[4] Bert U.W. Maes,[4] Valery N. Charushin,[1,2] and Oleg N. Chupakhin[1,2]*

[1] *Ural Federal University, 19 Mira Str., 620002 Ekaterinburg, Russia*

[2] *Institute of Organic Synthesis, Ural Branch of the Russian Academy of Sciences, 22 S. Kovalevskaya Str., 620990 Ekaterinburg, Russia.*

[3] *North Caucasus Federal University, 1 Pushkin Str., 355009 Stavropol, Russia*

[4] *Organic Synthesis Division, Department of Chemistry, University of Antwerp, 171 Groenenborgerlaan, 2020 Antwerp, Belgium*

*Corresponding author: chupakhin@ios.uran.ru

*Corresponding author: m.v.varaksin@urfu.ru

GRAPHICAL ABSTRACT:

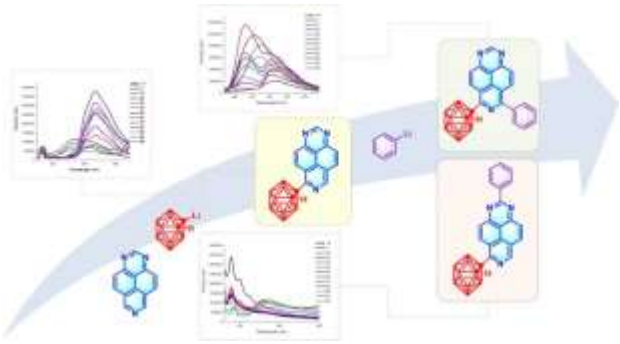

ABSTRACT:

A convenient transition metal-free approach, based on nucleophilic substitution of hydrogen (S_N^H), for consecutive regioselective C-H functionalization of 1,3,7-triazapyrene scaffolds with carboranyllithium and phenyllithium is reported. The theoretical calculations disclosed highlight key features in the regioselectivity and mechanism of the investigated S_N^H transformations. The novel 1,3,7-triazapyrene-based *ortho*-carboranes obtained have a large potential for the field of molecular electronics as organic luminophores, which are characterised by the aggregation-induced emission (AIE) and dual-emission effects.

Key words: carboranes, triazapyrene, nucleophilic substitution of hydrogen, photoluminescent materials, aggregation induced emission

INTRODUCTION

Organic luminescent materials attract considerable interest due to their versatile opportunities for the design of optoelectronic devices, such as organic light-emitting diodes (OLEDs),[1] organic field-effect transistors (OFETs),[2] light-emitting electrochemical cells (LEC),[3] solar cells,[4] flat-panel displays,[5] optical sensors,[6] and also as fluorescent labels for living systems.[7] One of the central obstacles, which hampers the wide utilization of these materials, is related to the decrease and/or quenching of the photoluminescence in concentrated solutions or in the solid state, also known as the Aggregation Caused Quenching (ACQ) effect.[8] Interestingly, the Aggregation Induced Emission (AIE) phenomenon, first reported in 2001,[9] is one of the possible solutions to overcome this ACQ problem. The AIE effect is based on the restriction of intramolecular movement (including rotation and vibration), thereby inhibiting non-radiative decays, resulting in a high fluorescence emission. Various types of AIE-active molecules have been reported, which includes functional derivatives of poly(hetero)cyclic compounds, polymers, and organometallic complexes.[10]

Recently, photoactive organoboron compounds, in particular functional derivatives of carboranes (*e.g.*, $C_2B_{10}H_{12}$), received renewed attention as organic fluorophores.[11] Due to the excellent suppression of ACQ, the *ortho*-carborane moiety is an attractive entity to construct solid state luminescent materials with advanced photophysical characteristics.[12] Moreover, one can find the diverse applications of carborane-based materials in catalysis,[13] medicine,[14] neutron detection and photovoltaics.[15] The majority of these carborane-containing compounds are boron clusters attached to polycyclic aromatic hydrocarbons (PAHs), which are well-proven as advanced photoactive materials.[12,16] At the same time, incorporation of heteroatoms containing a lone pair (*e.g.*, nitrogen) in the structure of the arene-moiety turns out to have a beneficial influence on the overall photoluminescence properties of boron-enriched compounds. This characteristic could be attributed to the specific electronic and spatial effects that take place between the azaheteroarene and carborane moieties *via* intra- and intermolecular hydrogen bonds. In addition, the energy gap between the electronic states is diminished because of the higher electron density of heterocyclic carborane molecules.[17]

Among the condensed polycyclic azaarenes, the molecular systems based on azapyrenes (Figure 1) appear to be of particular interest since the inclusion of nitrogen atoms into the pyrene framework not only affects the electronic characteristics (affording organic semiconductors,[18] redox-active molecules[19] and key building blocks of molecular machines[20]), but also the biological properties providing opportunities to be used as DNA intercalators[21] and as antitumor compounds.[22] However, the state of the art is lacking a general approach to produce functionalized azapyrenes derivatives with various architectures, which limits widespread distribution of azapyrenes.[18a,23] Notably, among the family of azapyrenes, 1,3,7-triazapyrenes and their functional derivatives are still particularly poorly studied. Unsubstituted and carbon-substituted 1,3,7-triazapyrenes (**3**) can be synthesized by heating pyrimidines with 1,3,5-triazines in polyphosphoric acid (PPA) (Scheme 1, Route A).[24] However, though very useful to make 1,3,7-triazapyrene itself, the substituent type that can be introduced *via*

this method is rather limited. The reaction of 1,3,7-triazapyrene (**3**) with electron-rich arenes in concentrated hydrochloric acid yields a limited amount of 6-aryl-1,3,7-triazapyrenes (Scheme 1, Route B).[25] Oxidative nucleophilic alkoxylation (Scheme 1, Route C)[26] and (alkyl)amination (Scheme 1, Routes D[27] and E[28]) have also been examined to deliver C(6)-heterosubstituted 1,3,7-triazapyrenes. Interestingly, only the C(6)-regioisomer has been obtained for those examples. Other functionalizations of the 1,3,7-triazapyrene (**3**) scaffold have not been examined to the best of our knowledge and the introduction of aliphatic substituents has been limited to methyl. In this manuscript, a convenient synthetic approach towards bulky aliphatic carborane(**1**)-containing derivatives of 1,3,7-triazapyrenes (**3**) is reported, combining the electronic characteristics of carboranes and azapyrenes, as well as photophysical studies of these novel luminophores (Scheme 1, Route F).

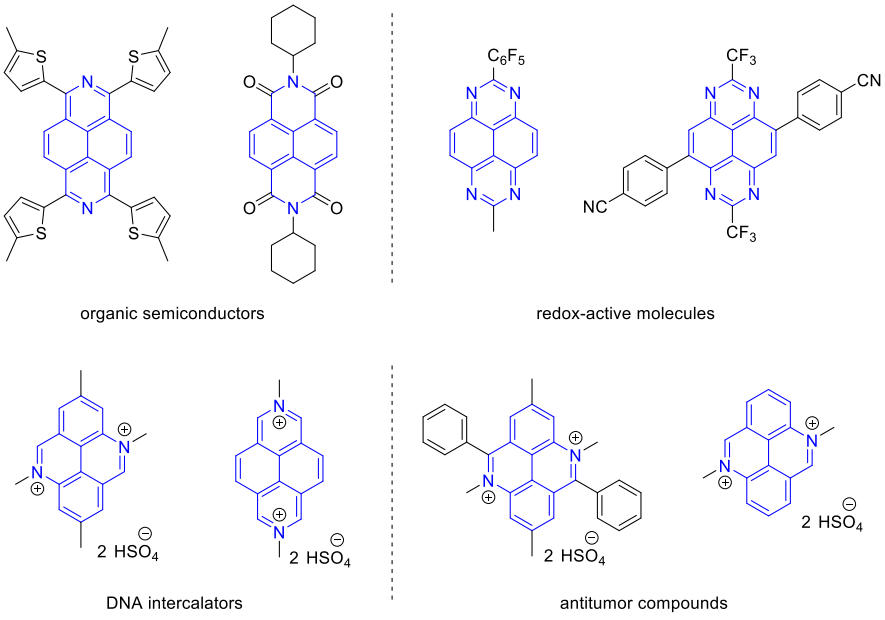

Figure 1. Examples of practically useful azapyrenes.

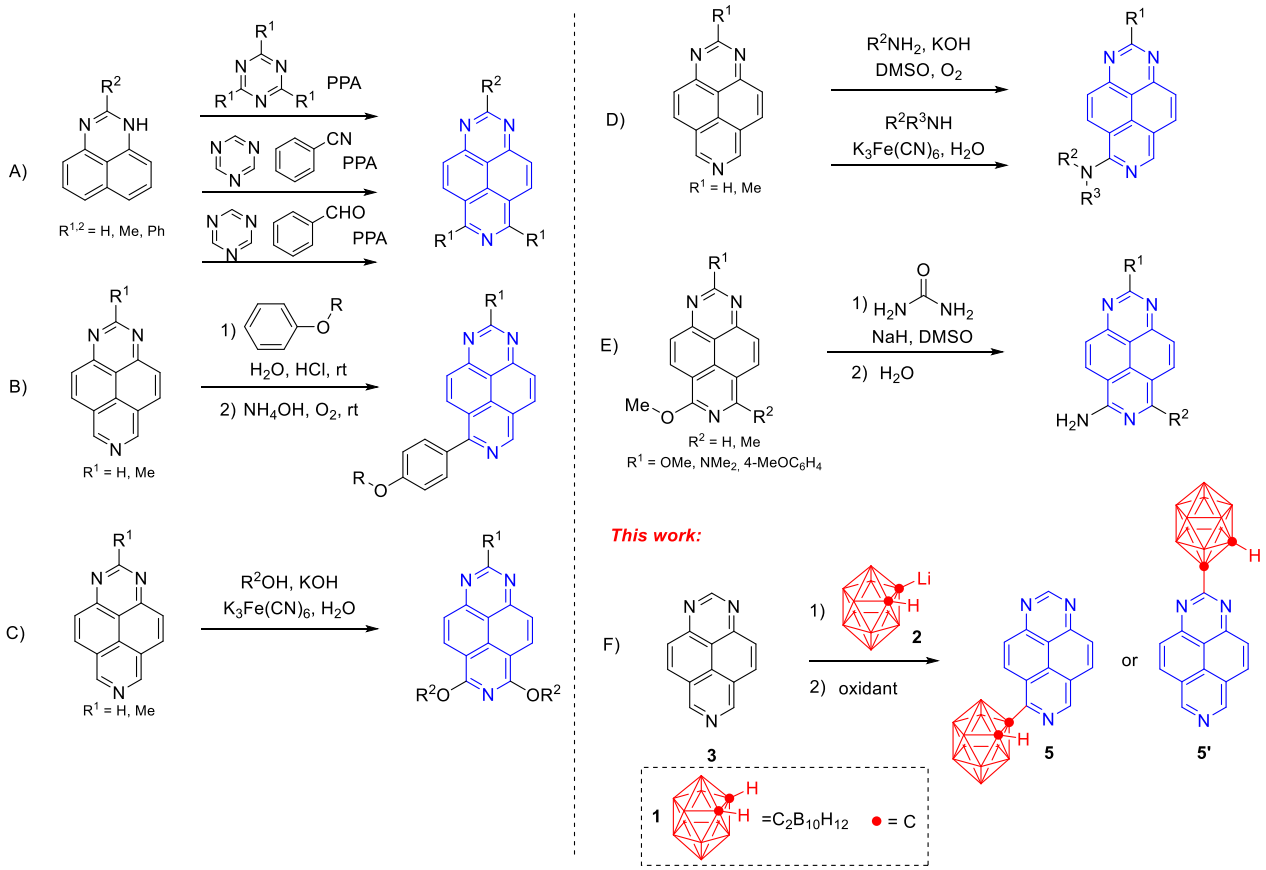

Scheme 1. State of the art (A-E) and envisioned C-H functionalization of 1,3,7-triazapyrene (**3**) with organolithiums (**2**).

RESULTS AND DISCUSSION

Coupling of 1,3,7-triazapyrene (3) with carboranyllithium (2)

The direct C-H functionalization[29] of 1,3,7-triazapyrene (**3**) with organolithiums *via* nucleophilic substitution of hydrogen (S_N^H reaction)[30] was studied as it neither requires preliminary installation of a leaving group, nor catalysis by transition metals. In particular, the reaction of 1,3,7-triazapyrene (**3**) with carboranyllithium (**2**), generated *in situ* from *n*-BuLi and *o*-carborane (**1**),[31] was investigated (Scheme 1 and Table 1). This C(sp^2)-H functionalization proceeds in two stages. Initially, nucleophilic reactant **2** is added to the azomethine (–CH=N–) bond of **3** to form the anionic σ^H-adduct **4**. Subsequent rearomatization of intermediate **4**, delivers stable S_N^H product **5**. The rearomatization

of the triazapyrene moiety requires an external oxidant for rearomatization and the reaction can therefore be classified as an oxidative S_N^H.[32]

A screening of the reaction conditions (reactants ratio, oxidizing agent, exposure time after the addition of the oxidant and temperature) to obtain 1-(1,3,7-triazapyrene-6-yl)-1,2-dicarba-*closo*-dodecaborane (**5**) or its regioisomer 1-(1,3,7-triazapyrene-2-yl)-1,2-dicarba-*closo*-dodecaborane **5'** was carried out (Table 1). Air only gave traces of **5** (Table 1, Entries 1-3), while the yield was considerably improved with 2,3-dichloro-5,6-dicyano-1,4-benzoquinone (DDQ) as an oxidant (Table 1, Entries 4-5). Reflux gave a better result than performing the reaction mixture at room temperature (Table 1, Entries 5 and 6). Alteration of the oxidant loading or the reaction time did not lead to a higher yield of **5** (Table 1, Entries 11). Finally, chloranils were not successful as oxidants for this transformation (Table 1, Entries 12-13). It should also be noted that there were no side products found, unreacted starting materials, namely, 40% of unreacted carborane **1** and 42% of the starting triazapyrene **3** being recovered.

Table 1. Optimization of the reaction conditions for the coupling of 1,3,7-triazapyrene (**3**) with carboranyllithium (**2**).

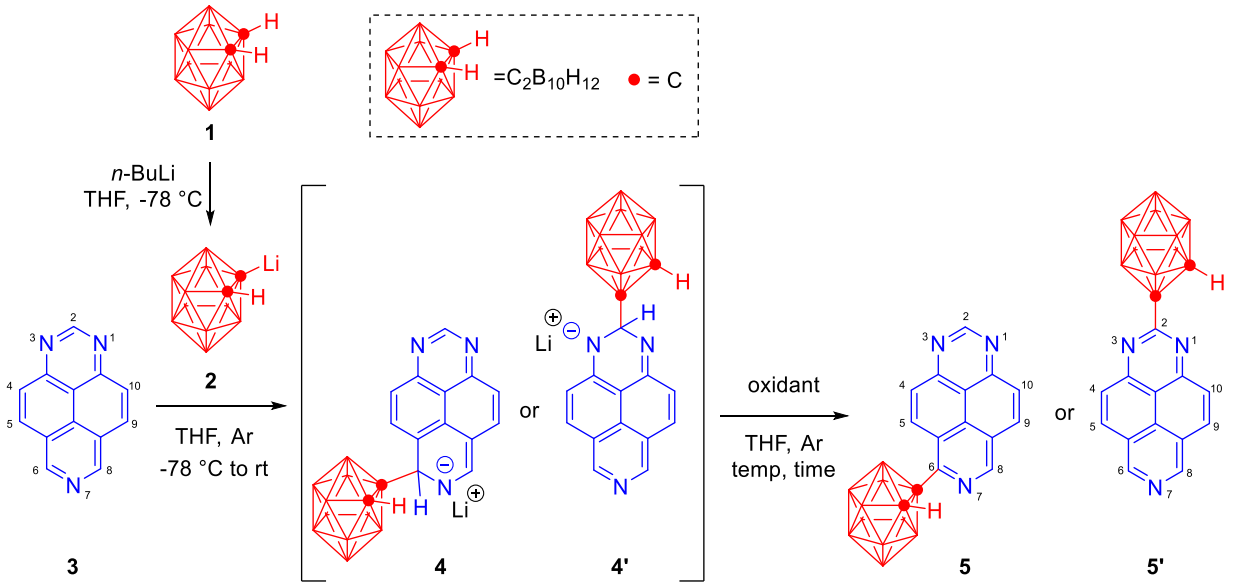

Entry	3 (equiv)	Oxidant[b] (equiv)	Temperature (°C)[c]	Time (h)[d]	Yield 5 (%)[e]	Yield 5' (%)
1	1.1	O_2 (air)	RT	1	<5	0
2	1.1	O_2 (air)	RT	2	<5	0
3	1.1	O_2 (air)	RT	3	8	0
4	1.1	DDQ (1.5)	RT	2	17	0
5	1.1	DDQ (1.5)	RT	3	21	0
6	**1.1**	**DDQ (1.5)**	**Reflux**	**3**	**35**	**0**
7	1.1	DDQ (1.2)	Reflux	3	26	0
8	1.1	DDQ (2.0)	Reflux	3	35	0
9	1.0	DDQ (1.5)	Reflux	3	24	0
10	1.2	DDQ (1.5)	Reflux	3	35	0
11	1.1	DDQ (1.5)	Reflux	4	35	0
12	1.1	*o*-chloranil (1.5)	Reflux	3	<5	0
13	1.1	*p*-chloranil (1.5)	Reflux	3	<5	0

[a] The reaction was carried out in dry THF (0.5 M) using carboranyllithium (2) prepared from *o*-carborane (1.0 equiv) and *n*-BuLi (1.1 equiv) at −78 °C.
[b] Oxidant was added to the reaction mixture at room temperature; DDQ = 2,3-dichloro-5,6-dicyano-1,4-benzoquinone, *o*-choranil = 3,4,5,6-tetrachloro-1,2-benzoquinone, *p*-choranil = 2,3,5,6-tetrachloro-1,4-benzoquinone.
[c] The temperature at which the reaction mixture was stirred after addition of the oxidant.
[d] Exposure time after addition of the oxidant.
[e] Isolated yield.

Despite the presence of two positions active for nucleophilic attack in 1,3,7-triazapyrene (C(2) and C(6)), interestingly only one single regioisomer (C(6)) has been isolated (Table 1). To investigate the regioselectivity of this reaction, first the Fukui function for nucleophilic attack (f^+) on **3** was calculated using Density Functional Theory (DFT) (see Figure S27). This calculation showed that 1,3,7-triazapyrene (**3**) is most susceptible for a nucleophilic attack at C(6) compared to C(2), which is

in accordance with the experimental results. Since the Fukui function is based on the molecular electron density and for example does not take steric effects in the transition states into account, the regioselectivity was further investigated by calculating the free energy profile of the reaction mechanism using DFT (Figure 2). The solid green line shows the reaction pathway when carboranyllithium (**2**) attacks 1,3,7-triazapyrene (**3**) at the C(6)-position. The first transition state (TS 1) corresponds to the σ^H-adduct **4** (intermediate). This TS 1 for the addition at C(6) is $\Delta^{\ddagger}G^{\circ}$ = 16.0 kcal/mol, while this barrier at C(2) is $\Delta^{\ddagger}G^{\circ}$ = 18.6 kcal/mol. Comparing this first barrier (TS 1) of the two pathways reveals that a nucleophilic attack at C(6) is therefore $\Delta\Delta^{\ddagger}G^{\circ}$ = 2.5 kcal/mol lower in energy than the attack at C(2). There is thus a kinetic preference for the attack at C(6), which explains why only regioisomer **5** is experimentally formed. It should also be noted that the intermediate formed after addition at C(6) is more stable than that at C(2). The intermediate σ^H-adduct **4**, forms a pre-complex with oxidant DDQ by a parallel π–π stacking interaction from which oxidation subsequently takes place (TS 2) leading to product **5**.

The Li^+ cation present in the reaction mixture, can interact with the solvent as well as with the different nitrogen atoms of substrate **3**, or with the oxygen or nitrogen atoms in DDQ. For example, for TS 2, there are different coordination spheres of Li^+ possible (SI, Cartesian coordinates of all optimized structures), yet they are lower in energy than TS 1. Therefore, to verify our conclusion, also the free energy profiles of the reaction without the Li^+ counterion were computed as shown in Figure 2 (dotted lines). These calculations confirm that nucleophilic addition of **2** still exclusively occurs at the C(6)-position with TS 1 being 2.5 kcal/mol lower than the addition at C(2), once more in accordance with the regioselectivity of our reaction.

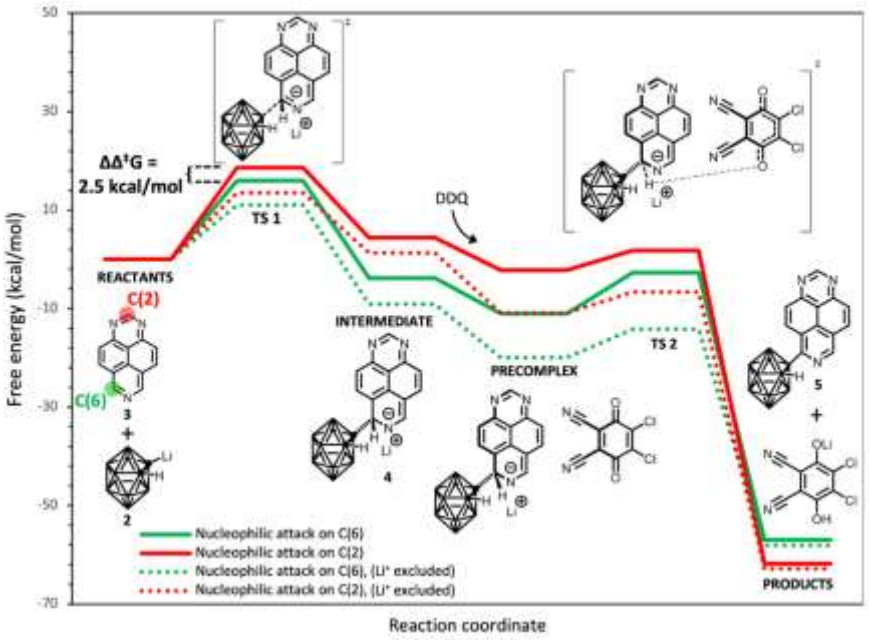

Figure 2. Free energy reaction profile for the reaction of carboranyllithium (**2**) with 1,3,7-triazapyrene (**3**) using DDQ as oxidant calculated at the IEFPCM/ωB97XD/6-311+G(2d) level of theory. The solid lines indicate that the Li^+ counterion was included in the calculations. The dotted lines correspond to the same respective free energy profiles, calculated without the Li^+ as counterion. The green lines indicate the attack of **2** on the C(6) of **3**; the red lines correspond to the attack of **2** at C(2).

Functionalization of 1,3,5-triazapyrene (3) *via* oxidative S_N^H

The obtained triazapyrenylcarborane **5** is a C(6) mono-substituted derivative still containing two azomethine moieties at C(2) and C(8) of the triazapyrene moiety that are theoretically accessible for the further oxidative S_N^H. Substituted triazapyrenylcarborane isomeric molecules are expected to possess different photophysical properties due to the variabilities in both electronic and spatial interactions between the triazapyrene core and the incorporated substituent. Functionalization of alicyclic pyrene at the C(1), C(3), C(6), and C(8) position was previously shown to result in significant red-shifts in the emission spectra of the obtained products, while substitution at the C(2) and C(7)

position had only a limited effect on the emission maximum.[33] It was also reported that the introduction of carborane in different positions of the pyrene affected the possibility of the free rotation of carborane, thereby changing the ratio of non-radiative decay and ICT-based radiation.[34] In addition, incorporation of aromatic fragments expanding the π-conjugated system of the molecule was demonstrated to improve the photophysical characteristics,[12,16a,35] providing the further fine tuning of the luminescent properties. Based on this, a further modification of **5** *via* S_N^H with phenyllithium as the coupling partner has been carried out (Scheme 2). While carboranyllithium **2** reacted selectively at C(6) of 1,3,7-triazapyrene (**3**), the coupling of **5** with PhLi occurs both on C(2) and C(8). Consequently, two regioisomers: 2-phenyl-1,3,7-triazapyrenyl-carborane (**8**) and 8-phenyl-1,3,7-triazapyrenyl-carborane **9** are isolated in 41% and 17% yield, respectively. Besides, up to 20% of starting triazapyrenylcarborane **5** can also be recovered to prepare the target bifunctionalized triazapyrenes.

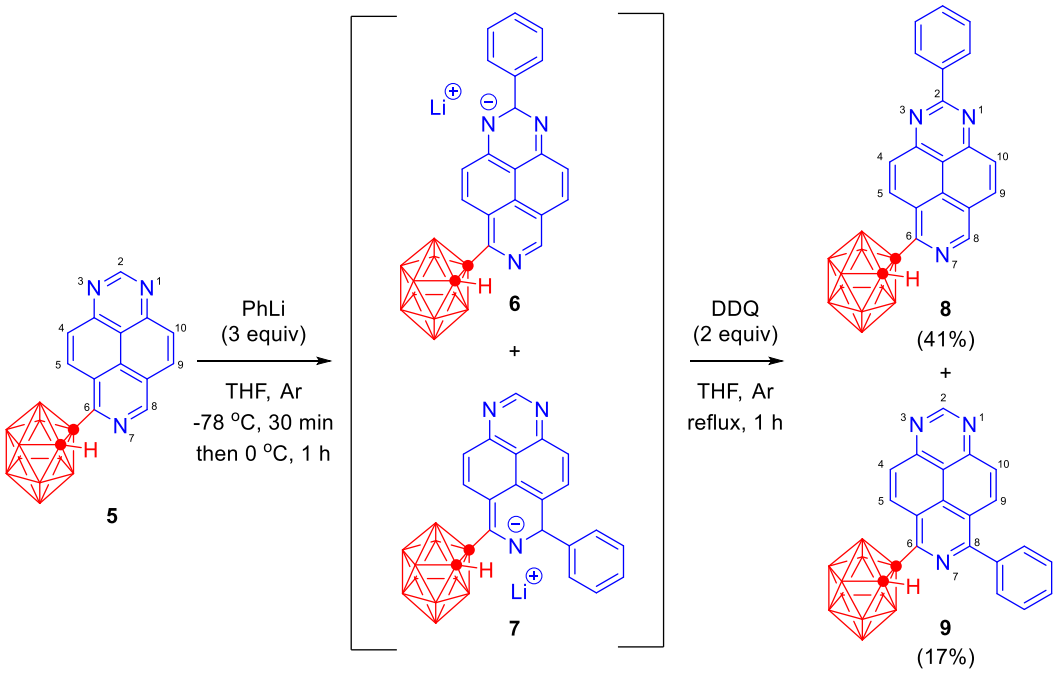

Scheme 2. Synthesis of regioisomers 1-(2-phenyl-1,3,7-triazapyrene-6-yl)-1,2-dicarba-*closo*-dodecaborane (**8**) and 1-(8-phenyl-1,3,7-triazapyrene-6-yl)-1,2-dicarba-*closo*-dodecaborane (**9**) from 1-(1,3,7-triazapyrene-6-yl)-1,2-dicarba-*closo*-dodecaborane (**5**).

To explain a mixture of regioisomers was obtained in this case, first the Fukui function for nucleophilic attack (f^+) was calculated with DFT (Figure S28). In this case, however, f^+ indicates a preference for a nucleophilic attack at C(8) compared to C(2). This is not in accordance with the experimental observation that both products **8** and **9** are formed. This could indicate that here steric interactions influence the transition states for the formation of the σ^H-adducts (TS 1). Therefore, the transition states for a nucleophilic attack on the two positions C(2) and C(8) of **5** were subsequently calculated with DFT (Figure 3). The barrier for the nucleophilic attack at C(2) is $\Delta^{\ddagger}G° = 15.4$ kcal/mol and $\Delta^{\ddagger}G° = 15.8$ kcal/mol for the attack at C(8). Both barriers are lower than the TS 1 of the coupling of **2** and **3** (Figure 2). Furthermore, the relative difference of $\Delta\Delta^{\ddagger}G° = 0.4$ kcal/mol is not a significant kinetic difference between the nucleophilic addition on carbon C(2) versus C(8) in the reaction of **5** with PhLi. As a result, both intermediates **6** and **7** are formed. This explains why both product **8** and **9** are obtained upon oxidation with DDQ. Since the energetic difference of 0.43 kcal/mol is within the error of the computational methodology, a more detailed interpretation of the results cannot be performed, *e.g.*, on the relative ratio of the products. Such an in-depth computational study would require, among other things, to include solvent molecules explicitly in the DFT calculations, which extends beyond the scope of this study. The Li^+ counterion affects the energy profiles here (compare the solid lines and the dotted lines in Figure 3). While the attack on C(8) is indicated by the Fukui function to be more susceptible to a nucleophilic attack, the coordination of the Li^+ ion by the N(7) in that transition state (TS 1), is sterically hindered by the carboranyl group. As a result, both C(8) and C(2) are almost equally susceptible for a nucleophilic attack by PhLi. The subsequent oxidation by DDQ occurs almost barrierless (TS 2).

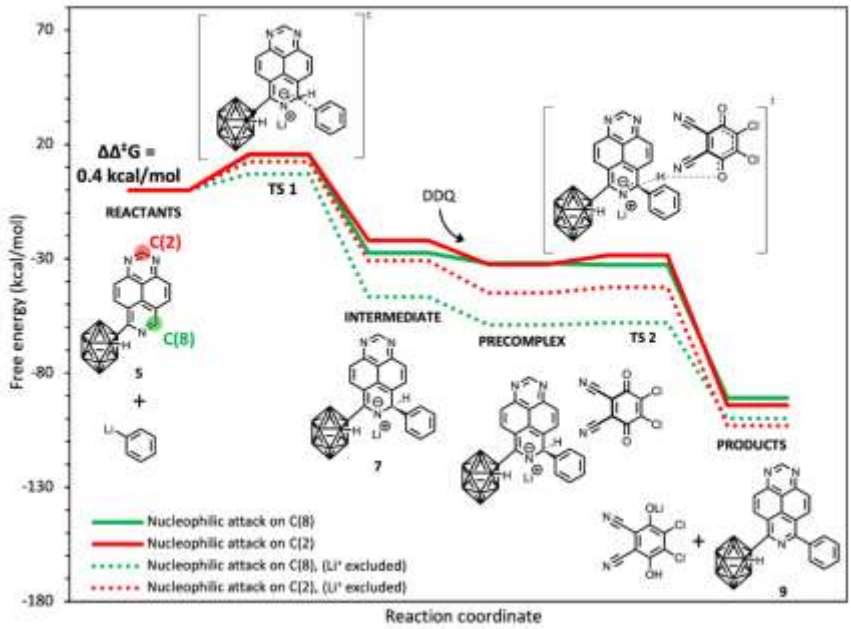

Figure 3. Free energy reaction profile of the reaction of phenyllithium with 1-(1,3,7-triazapyrene-6-yl)-1,2-dicarba-*closo*-dodecaborane (**5**) and DDQ as oxidant calculated at the IEFPCM/ωB97XD/6-311+G(2d) level of theory. The solid lines indicate that the Li^+ counterion was included in the calculations. The dotted lines correspond to the same respective free energy profiles, calculated without the Li^+ as counterion. The green lines indicate the attack of phenyllithium on the C(8) of **5**; the red lines correspond to the attack on C(2) of **5**.

Characterization of heterocyclic carboranes 5, 8, and 9

The synthesized triazapyrenylcarborane **5** and the phenyl-modified derivatives **8** and **9** were fully characterized *via* elemental analysis, IR, NMR spectroscopy (^{1}H, ^{13}C{^{1}H} (APT), ^{11}B, ^{1}H-^{13}C HSQC, ^{1}H-^{13}C HMBC experiments), and mass spectrometry. The absorption bands corresponding to the stretching vibrations of carborane B–B atoms (ν = 721 - 735 cm^{-1}), B–H (ν = 2573 - 2587 cm^{-1}) and C–H (ν = 3051 - 3072 cm^{-1}) are observed in the IR spectra. In the ^{1}H NMR spectra of azaheterocyclic carboranes **5**, **8**, and **9**, the expected resonance signals of both carborane and heteroarene fragments are also observed. Particularly, the characteristic signals of substituted carborane are registered as two sets, namely ^{1}H singlet of C_{Carb}–**H** at δ 5.97 - 6.02 ppm and 10H broadened multiplets of B–H protons at δ 3.64 - 1.72 ppm. The resonance signals of triazapyrenyl and

phenyl moieties are presented as a set of singlets, doublets and multiplets at δ 9.96 - 7.59 ppm. In the ^{1}H NMR spectra of triazapyrenylcarborane **5** and phenyl-substituted derivatives **8** and **9**, one can observe two characteristic singlets of protons at the C(2) and C(8) positions of the triazapyrene moiety presented in the spectrum of **5** (Figure 4a), meanwhile solitary singlets at δ 9.36 ppm and δ 9.92 are presented in the spectra of **8** (Figure 4b) and **9** (Figure 4c) correspondingly. Notably, protons of phenyl fragment are found to resonate at δ 8.85 - 8.83 ppm (2H) and at δ 7.61 - 7.59 ppm (3H) in case of **8** (Figure 4b) and at δ 7.80 - 7.78 ppm (2H) and at δ 7.69 - 7.67 ppm (3H) in the spectrum of **9** (Figure 4c). The chemical shifts of protons attached to the unsubstituted carborane carbon C_{carb}–**H** are located in the field at δ 5.97 - 6.02 ppm, an insignificant shift to the stronger field is observed in case of compound **9**. In the ^{13}C NMR spectra of azinylcarboranes **5**, **8** and **9**, the resonance signals of the carbon nuclei attributed to the Ccarb–H are presented at δ 61.5 - 61.5 ppm and the ones associated with the triazapyrenyl moiety are located at δ 76.2 - 76.1 ppm. In the mass spectra for all carboranyltriazapyrenes, the corresponding molecular ion peaks $[M]^{+}$ are registered as well.

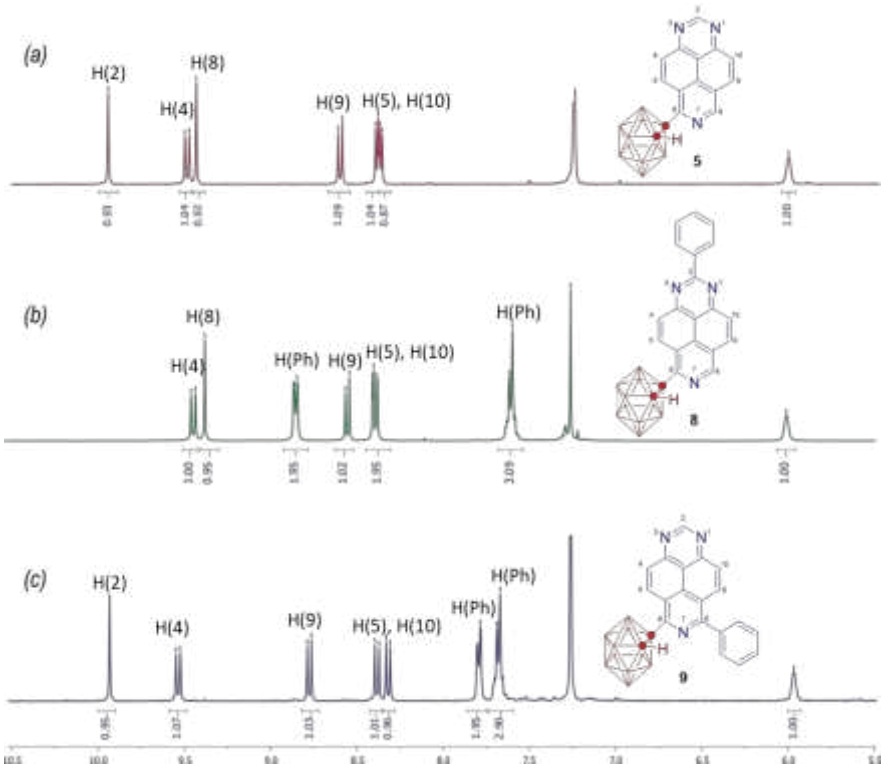

Figure 4. Comparative ^{1}H NMR (400 MHz) spectra of triazapyrenyl carboranes **5** *(a)*, **8** *(b)*, and **9** *(c)* in $CDCl_3$ at 295 K.

UV/Vis absorption spectroscopy of heterocyclic carboranes 5, 8, and 9

In order to evaluate the application potential of the carborane-modified 1,3,7-triazapyrenes as useful functional elements in the design of advanced optical materials, the photophysical properties have been studied. In particular, a preliminary assessment of photophysical characteristics was performed *via* UV-Vis absorption spectroscopy. Although unfunctionalized *ortho*-carborane is known to show extremely low absorbance,[17b] one can find interesting features in the absorption spectra of the synthesized heterocyclic carboranes **5**, **8** and **9** in the region of 250 - 400 nm (Figure 5). Additional studies of solvent effects on the UV-Vis absorption spectra for carboranes **5**, **8** and **9** have demonstrated no meaningfull "structure – properties" correlations (Figure S22), indicating that the ground state is not affected by the solvent polarity. The most distinct spectral differences comparing the spectra of the three compounds are the red-shift of the band at 356 nm in case of **9** compared with **5** and **8**, and the dominant band at 292 nm in the spectrum of **8.** To assign the main absorption bands of **5**, **8** and **9** and analyse the involved electronic transitions, TD-DFT calculations have been performed (see SI for details). The simulated spectra reproduce the experimental spectra very well (Figure 5B). It is worth noting that there is an expected arbitrary overestimation of the transition energies calculated with DFT, which should be taken into account when comparing with experiment.[36] Nonetheless, the relative spectral differences of **5**, **8** and **9** are reproduced in the simulated spectra. For example, the band at 356 nm in the experimental spectrum of **9** is at longer wavelengths compared to the same spectral regions in **5** and **8**, which is captured in the simulated spectra. Also, in the region 200 - 325 nm, the relative differences in the experimental spectra of the three compounds and the dominant band in the spectrum of **8**, are reproduced in the simulated spectra.

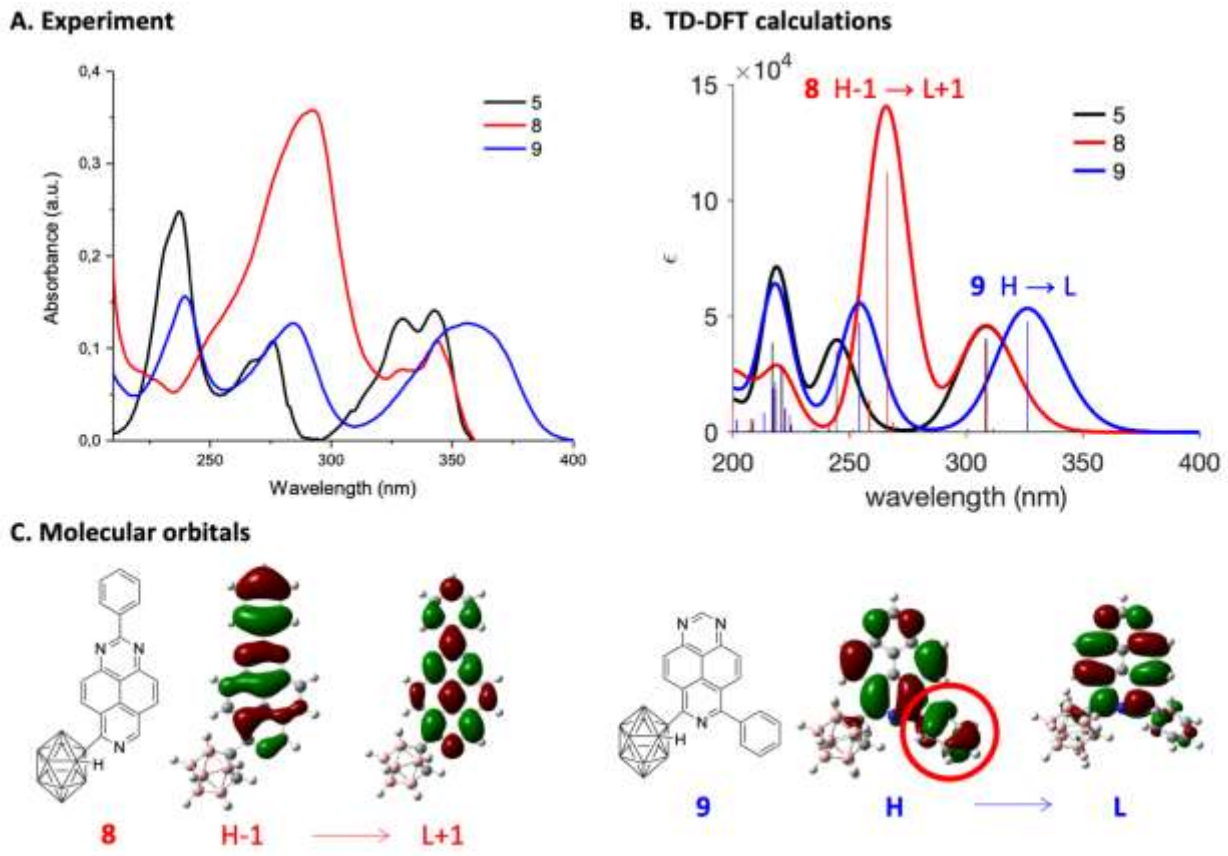

Figure 5. A. UV/Vis absorption spectra for heterocyclic carboranes **5**, **8** and **9** at a concentration of $1.0 \cdot \times 10^{-5}$ mol·L^{-1} in THF. The spectra were recorded at room temperature. B. TD-DFT computed absorption spectra (THF) of **5**, **8** and **9** (see more detail in the SI). C. Representations of the molecular orbitals involved in the dominant band of **8** and the low energy band of **9**.

The compositions of the electronic transitions involved in specific absorbance bands are listed in Table 2. The low energy bands in the spectra arise from transitions 5A, 8A and 9A, which are mostly composed of HOMO → LUMO. As shown in figure 5C and figure S28, these molecular orbitals (MOs) are delocalised on the 1,3,7-triazapyrene moiety. While the phenyl group of **8** is only limited involved in these MOs, the HOMO of **9** is delocalized on both the triazapyrene and the phenyl group. This difference of the frontier orbitals of **9** with those of **5** and **8** explains the lowest energy band in the spectrum of **9** to be at a lower energy relative to the bands of **5** and **8**.

The different position of the phenyl group in **8** and **9** affects the MOs as well as the orientation of this substituent. In **8** the phenyl group is in the same plane as the triazapyrene group, while the phenyl group of **9** is at an angle of 51° with the triazapyrene plane. The H-1 and L+1 of **8** are delocalized across this entire planar part of the molecule (Figure 5 C). The calculations show that the dominant band at 292 nm in the experimental spectrum of **8** arises from H-1 → L+1 (Table 2, entry 8B), and therefore differs from the MO transitions involved in the same spectral region of **5** and **9**, which have important contributions from other MOs as well (Table 2, entry 5B and 9B).

The higher energy UV bands (see, *e.g.*, C-D) arise from multiple more complex transitions. Overall, the spectral similarities and differences of **5**, **8** and **9** depend on the electronic structure of the triazapyrene group and how it is affected by the position of the phenyl substituent in **8** and **9**. Namely, the underlying nature and energy of the electronic transitions is different for each of the three isomers.

Table 2. Experimental and theoretical absorption maxima of **5**, **8** and **9**, main computed transitions and oscillator strengths, and the compositions in terms of molecular orbitals (HOMO (H) and LUMO (L)).[37] See more details and representations of the molecular orbitals in SI.

Entry	Experimental max (nm)	Theoretical max (nm)	Theoretical transition (nm)	Oscillator strength	Major contributions
5A	330	309	309	0.6272	HOMO→LUMO (92%)
5B	276	244	244	0.5479	H-1→LUMO (45%), HOMO→L+1 (47%)
5C	237	219	221	0.4446	H-3→L+1 (44%), H-1→L+1 (35%)
5D	237	219	217	0.5928	H-3→L+1 (27%), H-1→L+1 (49%)
8A	341	309	308	0.6092	HOMO→LUMO (90%)
8B	292	266	266	1.7260	H-1→L+1 (81%)
8C	-	219	218	0.2854	H-5→LUMO (59%), HOMO→L+2 (10%)

9A	355	326	326	0.7351	HOMO→LUMO (94%)
9B	284	254	254	0.7262	H-4→LUMO (14%), H-2→LUMO (35%), HOMO→L+1 (32%)
9C	240	218	218	0.3328	H-4→L+1 (18%), H-2→L+1 (15%), H-1→LUMO (15%)

Fluorescence spectroscopy of heterocyclic carboranes 5, 8 and 9

The fluorescence emission spectra for the obtained compounds have also been studied. As shown in Figure 6, structures of the emission spectra for compounds **5**, **8** and **9** are similar and demonstrate several emission bands with different intensities at 365 nm and in the range from 450 to 550 nm, probably related to local excitation (LE) states and intramolecular charge transfer (ICT) states, respectively. It is worth noting that the emission caused by the ICT state is significantly higher for phenyl-substituted derivative **9** and mono-substituted triazapyrene **5** in comparison with compound **8**, in which the contributions of LE and ICT emissions appear to be practically equal. At the same time, there is a blue-shift of the ICT-emission band compared with that for **5** and **9** to 70 nm in the emission spectrum of 2-phenyl-1,3,7-triazapyrenyl-carborane (**8**).

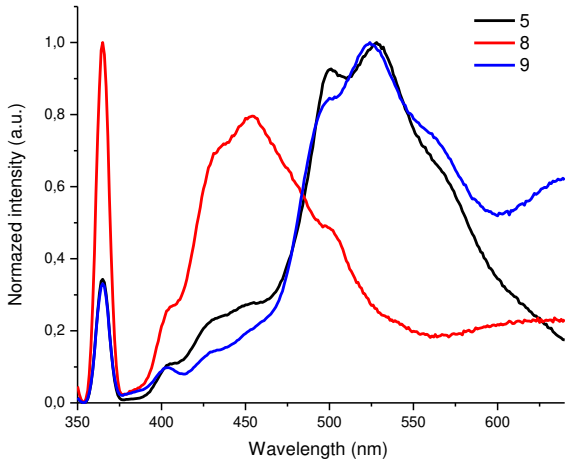

Figure 6. Normalized emission spectra for heterocyclic carboranes **5**, **8,** and **9**. Sample preparation: $1.0 \cdot \times 10^{-5}$ mol·L^{-1} in THF at room temperature; the excitation wavelength is 330 nm.

To gain insight in the emission mechanism that takes place in the triazapyrenyl-derived carboranes, the fluorescence spectra were recorded in four different solvents (THF, DCM, MeCN, and MeOH) (Figure 7). We report here that carboranyltryazapyrene **5** exhibits multiple emission behaviour in all solvents. Contribution to the LE state emission is higher in MeCN, while one can see the most intensive peaks corresponding to the ICT state in other solvents. It is noteworthy that maxima of ICT-related peaks can be registered from 458 to 528 nm depending on the solvent used. On the other hand, 8-phenyl-1,3,7-triazapyrenyl-carborane **8** demonstrates dual-emission behaviour with LE peaks at 380 nm in all solvents and structured ICT-peaks in THF and DCM, as well as a broadened emission band in MeCN and MeOH. At the same time, emission of 2-phenyl-1,3,7-triazapyrenyl-carborane **9** in THF is characterised with a strong broadened red-shifted band at 530 nm and very weak peak at 390 nm related to LE state. In addition also single broadened bands with maxima at 436 nm in DCM and MeOH can be observed, along with a dual-emissive behaviour in MeCN with structured LE-peak at 391 nm and broadened ICT-peak at 465 nm. One can conclude that incorporation of a phenyl substituent at the different positions of carboranyltriazapyrene **5** has a strong influence on its emission spectra, enabling one to tune the properties by activating emissions caused either by LE or ICT transitions.

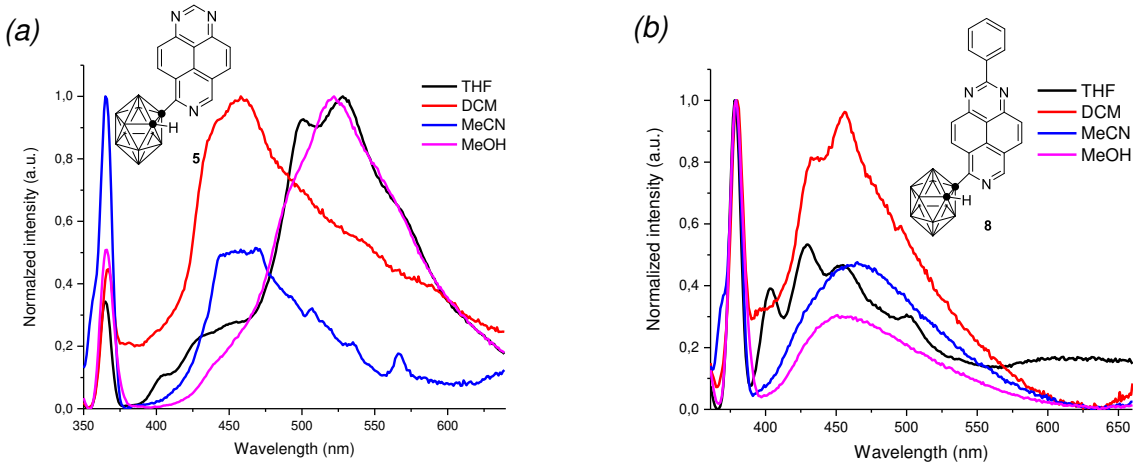

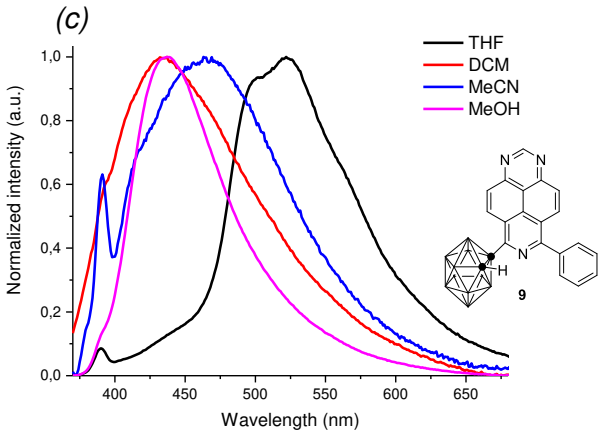

Figure 7. Normalized emission spectra for carborane-enriched derivatives **5** *(a)*, **8** *(b)*, and **9** *(c)*. Sample preparation: $1.0 \times \cdot 10^{-5}$ mol·L^{-1} in different solvents at room temperature; the excitation wavelength is 330, 341 and 350 nm respectively.

In addition, to evaluate the ICT character of emission the low temperature emission spectra for obtained structures were examined at 77 K in 2-MeTHF (Figure S25). At room temperature all compounds demonstrate only the LE state emission in 2-MeTHF solution, however at 77 K one can see ICT-based emission in the region of 550 nm to 630 nm. These results support that the growth of molecular rigidity, and suppressing molecular motions of carborane-containing molecules, leads to an increase in ICT-caused emission.

Subsequently, the aggregation emission properties for the synthesized azaheterocyclic carboranes were investigated. Changes in the fluorescence emission intensity were monitored by varying the water content in the THF solution (Figure 8). Augmentation of the water ratio results in an enhancement of the fluorescence intensity with a maximum at 50%, 99% and 70% of water content for compounds **5**, **8**, and **9**, respectively. Increasing the water content above 99%, led to a decrease of emission intensity for derivatives **5** and **9**. Notably, the similar up-down phenomenon had previously been reported in case of some fluorophore compounds possessing the AIE properties.[38]

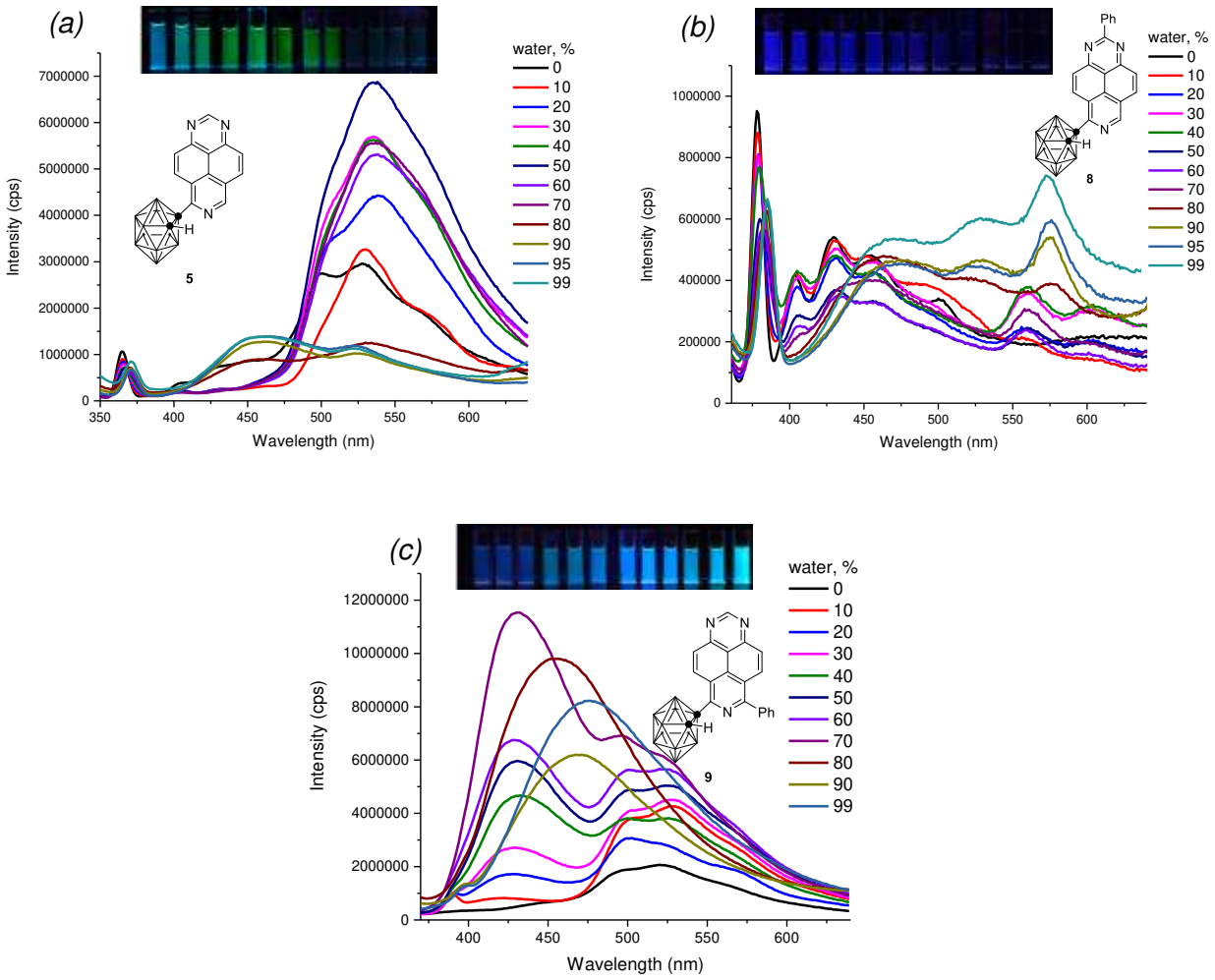

Figure 8. Fluorescence spectra of **5**, $\lambda_{ex} = 330$ nm *(a)*, **8**, $\lambda_{ex} = 341$ nm *(b)*, **9**, $\lambda_{ex} = 350$ nm *(c)* in THF/water mixtures with different water volume fractions, $c = 1.0 \times 10^{-5}$ mol·L^{-1}

Interestingly, in the fluorescence emission spectra of **9** a new emission band around 430 nm appears for suspensions containing 20% till 70% of water content in THF. This emission band demonstrates a red-shift when the water content in THF is further increased till 99%. A novel emission band around 450 nm is also observed in the emission spectra of **5** with water fractions beginning from 80%. The appearance of new emission bands seems to be attributed to the triazapyrenyl moieties leading to the excimer formation, because the quenching of ICT emission is observed with the

enhancement of this novel emission.[39] As far as the AIE properties of derivative **8** are concerned, one can see a decrease in emission intensity in case of samples with a water content from 10% to 70%. Beginning from the 80% of water fraction, the appearance of slightly structured broadened emission band from 450 to 600 nm is observed.

Cyclic voltammetry of heterocyclic carboranes 5, 8 and 9

Electrochemical properties of synthesized triazapyrenylcarboranes **5**, **8** and **9** were investigated by cyclic voltammetry (CV) under N_2 atmosphere using 5mM solution of analyzed compounds in anhydrous acetonitrile with 0.1 M Bu_4NPF_6 as the supporting electrolyte at a scan rate 100 mV/s. All measurements were performed using the standard three electrode cell: glassy carbon working electrode, $Ag/AgNO_3$ reference electrode and a carbon rod counter electrode. HOMO and LUMO energies were determined by cyclic voltammetry from the onset of oxidation and reduction peaks relative to ferrocene/ferricinium (Fc/Fc^+) with a known HOMO energy level of 4.8 eV[35a]:

$$E_{HOMO}\ (eV) = -\ [E_{ox\ onset} - E_{1/2}(Fc/Fc^+) + 4.8]$$

$$E_{LUMO}\ (eV) = -\ [E_{red\ onset} - E_{1/2}(Fc/Fc^+) + 4.8]$$

The recorded voltammograms show a pronounced irreversible anodic peak at 1.4 V – 1.5 V and one or two slight cathodic peaks between -0.5 V and -0.7 V (Figure 9). Based on these CVs, the HOMO and LUMO energy values were estimated (Table 3). HOMO energies of all three compounds 5, 8, 9 are close to -6 eV and LUMO energies of -4 eV were obtained. The calculation of the HOMO, LUMO and gap (E_g) with DFT strongly depends on the density functional that is used and the percentage of Hartree-Fock exchange included in it.[40] The functional ωB97XD that was used for the determination of the reaction mechanism has a relatively large percentage of Hartree-Fock exchange and is therefore not recommended for the calculation of the gap ($E_{g,calc}$).[40a] The $E_{g,calc}$ calculated for **5**, **8** and **9** with ωB97XD is above 7 eV (see table S4). Functionals with a lower percentage of Hartree-Fock exchange such as B3LYP or a pure functional without Hartree-Fock exchange BLYP result in much lower E_g

values, that are closer to experiment and are therefore more commonly used.[16a,35d,40,41] The often used B3LYP functional gives $E_{g,calc}$ values of 4.22 eV for **5** and **8** and 3.93 eV for **9** (see table S4). While B3LYP in other studies resulted in good agreement between experiment and theory,[16a,35d,40,41] in this case, BLYP gives $E_{g,calc}$ closest to the experiment with 2.60 eV, 2.58 eV and 2.36 eV for **5**, **8** and **8**, respectively (see table 3 and table S4).

Table 3. Estimated HOMO-LUMO energies for the compounds **5, 8, 9**[a]. The values in round brackets are calculated using BLYP/6-311+G(2d) with IEFPCM for acetonitrile. Results from other DFT levels are given in Table S5.

Compound	$E_{Ox\ onset}$	$E_{Red\ onset}$	E_{HOMO}	E_{LUMO}	E_g
	V	V	eV	eV	eV
5	1.40	-0.57	-5.98 (-6.05)	-4.01 (-3.45)	1.97 (2.60)
8	1.55	-0.55	-6.13 (-5.96)	-4.03 (-3.39)	2.10 (2.58)
9	1.50	-0.55	-6.08 (-5.79)	-4.03 (-3.43)	2.05 (2.36)

[a] Recorded with 0.1 M Bu_4NPF_6 as electrolyte in acetonitrile (5 mM) at room temperature with scan rate: 100 mV/s. Potentials are expressed as the half-wave potentials ($E_{1/2}$) in V vs $Ag/AgNO_3$. For all compounds using ferrocene as an internal reference

(a) *(b)*

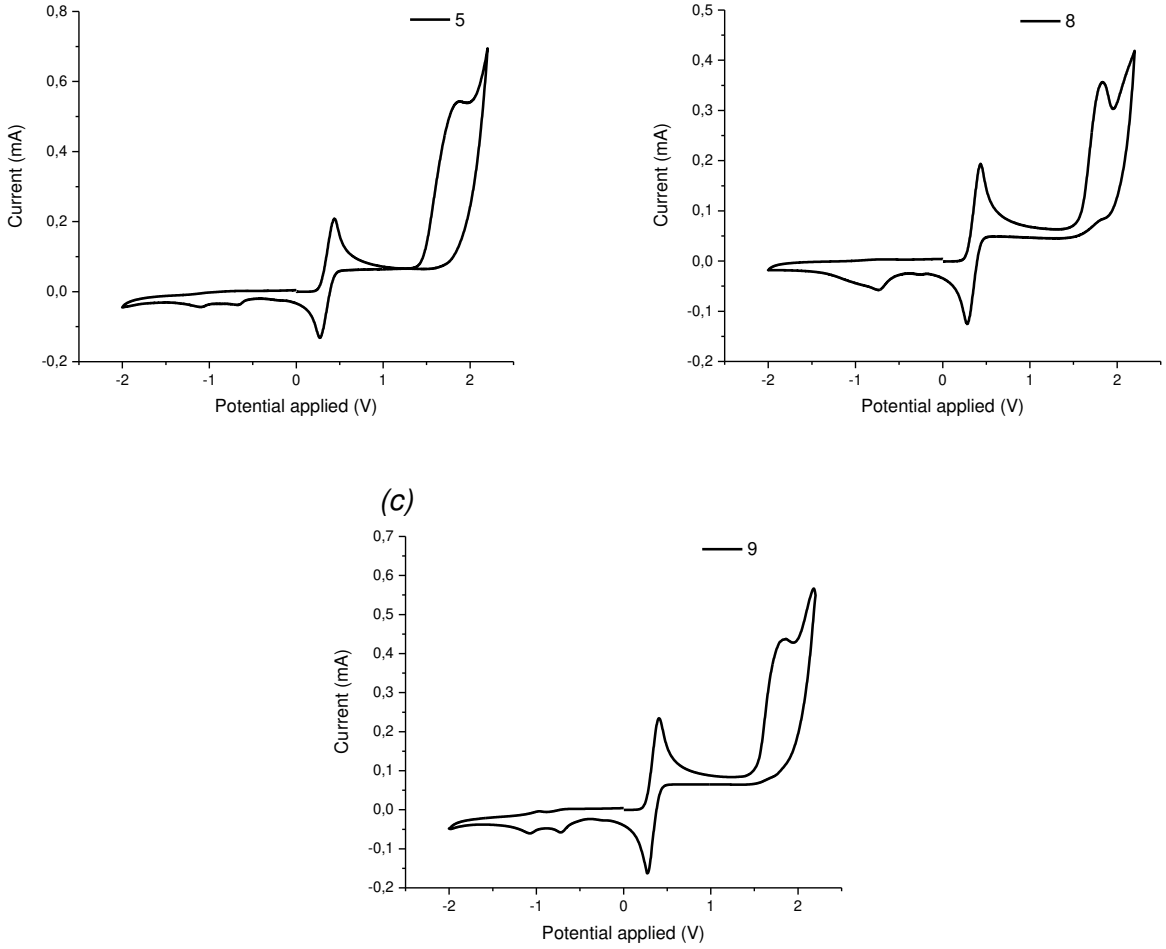

Figure 9. Cyclic voltammograms of **5** *(a)*, **8** *(b)*, **9** *(c)*. Sample preparation: 5.0×10^{-3} mol·L^{-1} in N_2 saturated anhydrous acetonitrile with Bu_4NPF_6 (0.1 mol·L^{-1}) as supporting electrolyte. A glassy carbon electrode and carbon rod served as the working and counter electrode, respectively. $Ag/AgNO_3$ was employed as reference electrode. Scan rate: 100 mV/s.

CONCLUSIONS

In summary, an oxidative S_N^H methodology has been developed providing an effective tool to functionalize 1,3,7-triazapyrene with carboranyl and phenyl moieties. DFT calculations enabled one to gain insight in the mechanism and regioselectivity of this oxidative S_N^H transformation, which have poorly been studied before. Mono and double C-H functionalization of the 1,3,7-triazapyrene

scaffolds afforded unknown boron-enriched polyazaheterocyclic hydrocarbons with the dual-emissive behaviour and AIE-properties. The revealed fluorescent characteristics allow the obtained azinylcarboranes to be considered as prospective functional elements in the design of advanced organic luminescence materials.

EXPERIMENTAL SECTION

General experimental methods

The ^{1}H NMR (400 MHz), ^{13}C NMR (100 MHz), ^{11}B (128 MHz) spectra were recorded using TMS as the internal standard and $CDCl_3$ as a deuterated solvent. The mass spectra were recorded on a mass spectrometer with sample ionization by electron impact (EI). The IR spectra were recorded using a Fourier-transforminfrared spectrometer equipped with a diffuse reflection attachment. The elemental analysis was carried out on a CHNS/O analyzer. The reactions were monitored by analytical TLC on Sorbfil UV-254 aluminum foil plates with 0.2 mm silica gel with a fluorescent indicator visualized under UV light. Column chromatography was performed on silica gel (60, 0.040-0.063 mm (230-400 mesh)).

The UV–Vis and fluorescence spectra were recorded at 25 °C using a Shimadzu UV-1800 spectrophotometer and HoribaFluoromax-4 Spectrofluorometer. The reactions were monitored by analytical TLC on Sorbfil UV-254 aluminum foil plates with 0.2 mm silica gel with a fluorescent indicator visualized under UV light. Melting points were determined on Stuart SMP10 melting point apparatus and are uncorrected.

Solvents for optical studies: dichloromethane (DCM), acetonitrile (MeCN), tetrahydrofuran (THF), methanol (MeOH) were purchased at pure or extra pure quality and used without additional purification. *n*-BuLi (1.6 M solution in hexane), 2,3-dichloro-5,6-dicyano-1,4-benzoquinone (DDQ), phenyl lithium were purchased from Sigma-Aldrich. 1,3,7-triazapyrene[24a] was prepared according to the published procedures.

General method for the synthesis of C-modified carborane 5

A flame-dried Schlenk flask equipped with a stirr barr, was cooled to room temperature under argon. Subsequently it was charged with 1,2-*closo*-carborane **1** (1.39 mmol, 200 mg, 1.0 equiv) in THF (3.0 mL, dry) at -78 °C. To this vigoriously stirred solution, *n*-BuLi (1.6 M in hexane, 1.53 mmol, 0.955 mL, 1.1 equiv) was added. The mixture was stirred at -78 °C for 30 min, then was warmed up to 0 °C and stirred for additional 1 h. The mixture was cooled to –78 °C and a solution of 1,3,7-triazapyrene (**3**, 1.53 mmol, 313 mg, 1.1 equiv) in THF (20 mL, dry) was added. The resulting solution was allowed to warm up to ambient temperature and was stirred for 15 min. Then a solution of DDQ (2.08 mmol, 473 mg, 1.5 equiv) in THF (5.0 mL, dry) was added and the resulted mixture was refluxed for 3 h under argon. The reaction mixture was subjected to neutral aluminia column chromatography with the chloroform as an eluent, the resulting eluate was concentrated to dryness *in vacuo* and the residue was subjected to silica gel column chromatography with the chloroform – hexane mixture as an eluent, the resulting eluate was concentrated to dryness under reduced pressure.

1-(1,3,7-Triazapyrene-6-yl)-1,2-dicarba-*closo*-dodecaborane (5)

Yield 168 mg (35 %), mp >240 °C, R_f 0.4 (hexane/EtOAc, 8:2).^{1}H NMR (400 MHz, $CDCl_3$, δ): 9.96 (s, 1H), 9.50 (d, *J* = 9.88 Hz, 1H), 9.45 (s, 1H), 8.62 (d, *J* = 9.20 Hz, 1H), 8.45-8.30 (m, 2H), 6.02 (s, 1H, C(B)-H), 3.28-1.89 (m, 10H, B-H). ^{13}C NMR (100 MHz, $CDCl_3$, δ): 158.66 (CH), 155.09 (C), 154.05 (C), 145.88 (CH), 133.86 (CH), 133.14 (CH), 130.28 (CH), 129.80 (CH), 127.81 (C), 124.80 (C), 121.46 (C), 115.43 (C), 76.10 (C(B)), 61.50 (C(B)-H). ^{11}B NMR (128 MHz, $CDCl_3$, δ): -1.75 (d, *J* = 130.08 Hz, 1B), -3.39 (br s, 1B), -7.65 (d, *J* = 155.77 Hz, 2B), -9.06-(-12.06) (m, 4B), -13.37 (d, *J* = 172.49 Hz, 2B). IR (DRA, *v*): 3052, 2573, 1681, 1624, 1585, 1553, 1500, 1381, 1265, 1202, 1141, 1014, 914, 853, 798, 744, 721, 643 cm^{-1}. MS (EI) *m/z*: $[M]^+$ Calcd for $C_{15}H_{17}N_3B_{10}$: 347; Found: 347. Anal. Calcd for $C_{15}H_{17}N_3B_{10}$: C, 51.86; H, 4.93; B, 31.11; N, 12.10. Found: C, 51.82; H, 4.87; B, 31.03; N, 12.28.

General method for the synthesis of C-modified carboranes 8 and 9

A flame-dried Schlenk flask equipped with a stirr barr, was cooled to room temperature under Argon. Subsequently it was charged with 1-(1,3,7-triazapyrene-6-yl)-1,2-dicarba-*closo*-dodecaborane **5** (0.29 mmol, 100 mg, 1.0 equiv) in THF (7 mL, dry) at -78 °C. To this vigoriously stirred solution, PhLi (1.8 M in dibutyl ether, 0.87 mmol, 0.48 mL, 3.0 equiv) was added. The mixture was stirred at -78 °C for 30 min, then was warmed up to 0 °C and was stirred for additional 1 h. The mixture was cooled to –78 °C and a solution of DDQ (0.57 mmol, 130 mg, 2.0 equiv) in THF (2 mL, dry) was added and the resulted mixture was refluxed for 1 h under argon. The reaction mixture was subjected to neutral aluminia column chromatography with the chloroform as an eluent, the resulting eluate was concentrated to dryness in vacuo and the residue was subjected to silica gel column chromatography with the chloroform–hexane mixture as an eluent, the resulting eluate was concentrated to dryness under reduced pressure.

1-(2-Phenyl-1,3,7-triazapyrene-6-yl)-1,2-dicarba-*closo*-dodecaborane (8)

Yield 50 mg (41 %), mp >240 °C, R_f 0.5 (hexane/EtOAc, 8:2).^{1}H NMR (400 MHz, $CDCl_3$, δ): 9.43 (d, *J* = 9.80 Hz, 1H), 9.36 (s, 1H), 8.90-8.77 (m, 2H, Ph), 8.54 (d, *J* = 9.16 Hz, 1H), 8.44-8.33 (m, 2H), 7.67-7.52 (m, 3H, Ph), 6.02 (s, 1H, C(B)-H), 3.54-1.72 (m, 10H, B-H). ^{13}C NMR (100 MHz, $CDCl_3$, δ): 164.66 (C), 155.74 (C), 154.67 (C), 145.65 (CH), 145.52 (C), 138.32 (C), 133.58 (CH), 132.81 (CH), 131.47 (CH), 130.64 (CH), 130.18 (CH), 129.39 (CH), 128.99 (CH), 128.08 (C), 124.72 (C), 121.33 (C), 113.91 (C), 76.24 (C(B)), 61.48 (C(B)-H). ^{11}B NMR (128 MHz, $CDCl_3$, δ): 0.13-(-4.60) (m, 2B), -7.74 (d, *J* = 157.27 Hz, 2B), -8.93-(-12.21) (m, 4B), -13.33 (d, *J* = 154.66 Hz, 2B). IR (DRA, *v*): 3072, 2573, 1628, 1587, 1465, 1396, 1309, 1240, 1013, 916, 832, 800, 724, 690, 615 cm^{-1}. MS (EI) *m/z*: $[M]^+$ Calcd for $C_{21}H_{21}N_3B_{10}$: 423; Found: 423. Anal. Calcd for $C_{21}H_{21}N_3B_{10}$: C, 59.56; H, 5.00; B, 25.52; N, 9.92. Found: C, 59.81; H, 5.22; B, 25.19; N, 9.78.

1-(8-Phenyl-1,3,7-triazapyrene-6-yl)-1,2-dicarba-*closo*-dodecaborane (9)

Yield 21 mg (17 %), mp >240 °C, R_f 0.6 (hexane/EtOAc, 8:2).^{1}H NMR (400 MHz, $CDCl_3$, δ): 9.92 (s, 1H), 9.53 (d, *J* = 9.72 Hz, 1H), 8.77 (d, *J* = 9.44 Hz, 1H), 8.37 (d, *J* = 9.76, 1H), 8.31 (d, *J* = 9.56 Hz, 1H), 7.88-7.58 (m, 5H, Ph), 5.96 (s, 1H, C(B)-H), 3.64-1.76 (m, 10H, B-H). ^{13}C NMR (100 MHz, $CDCl_3$, δ): 158.58 (CH), 155.47 (C), 154.66 (C), 154.34 (C), 144.88 (C), 137.75 (C), 134.24 (CH), 133.19 (CH), 131.08 (CH), 129.96 (CH), 129.80 (CH), 129.37 (CH), 129.14 (CH), 122.35 (C), 120.57 (C), 115.93 (C), 76.11 (C(B)), 61.46 (C(B)-H). ^{11}B NMR (128 MHz, $CDCl_3$, δ): 0.41-(-6.01) (m, 2B), -7.82 (d, *J* = 149.36 Hz, 2B), -9.11-(-12.26) (m, 4B), -13.57 (d, *J* = 162.84 Hz, 2B). IR (DRA, *v*): 3051, 2954, 2918, 2850, 2587, 1730, 1622, 1462, 1377, 1264, 1180, 1014, 798, 735, 698, 606 cm^{-1}. MS (EI) *m/z*: $[M]^+$ Calcd for $C_{21}H_{21}N_3B_{10}$: 423; Found: 423. Anal. Calcd for $C_{21}H_{21}N_3B_{10}$: C, 59.56; H, 5.00; B, 25.52; N, 9.92. Found: C, 59.81; H, 5.23; B, 25.14; N, 9.82.

Notes

The authors declare no conflict of interest.

ASSOCIATED CONTENT

Supporting Information.

The Supporting Information is available free of charge at

Full experimental details and characterization data are given in the Supporting Information.

ACKNOWLEDGEMENTS

The research was financially supported by the Russian Science Foundation (Project no. 20-43-01004), a bilateral Russian Science Foundation (RSF) – Fund for Scientific Research Flanders (FWO) project, and the Francqui Foundation. The Flemish Supercomputing Center (VSC) is acknowledged for providing computational resources.

REFERENCES

(1) (a) Pode, R. Organic light emitting diode devices: An energy efficient solid state lighting for applications. *Renew. Sustain. Energy Rev.* **2020**, *133*, 110043; (b) Okada, H.; Naka, S. Mixed single-layer and self-alignment technology of organic light-emitting diodes and multi-functional integration in organic devices. *Jpn. J. Appl. Phys.* **2020**, *59*, SO0802; (c) Negi, S.; Mittal, P.; Kumar, B. In-Depth Analysis of Structures, Materials, Models, Parameters, and Applications of Organic Light-Emitting Diodes. *J. Electron. Mater*. **2020**, *49*, 4610-4636; (d) Li, Z. Ed.: *Organic Light-Emitting Materials and Devices (2nd ed.)*, CRC Press, Boca Raton, **2015**.

(2) (a) Muccini, M.; Toffanin, S. *Organic Light-Emitting Transistors: Towards the Next Generation Display Technology*, Wiley, New York, **2016**, 288 p.; (b) Kim, M.; Ryu, S. U.; Park, S. A.; Choi, K.; Kim, T.; Chung, D.; Park, T. Donor–Acceptor-Conjugated Polymer for High-Performance Organic Field-Effect Transistors: A Progress Report. *Adv. Funct. Mater*. **2020**, *30*, 1904545; (c) Yu, Y.; Ma, Q.-H.; Ling, H.-F.; Li, W.; Ju, R.-L.; Bian, L.-Y.; Shi, N.-E.; Qian, Y.; Yi, M.-D.; Xie, L.-H.; Huang, W. Small-Molecule-Based Organic Field-Effect Transistor for Nonvolatile Memory and Artificial Synapse. *Adv. Funct. Mater*. **2019**, *29*, 1904602; (d) Moser, M.; Ponder, J. F.; Wadsworth, A.; Giovannitti, A.; McCulloch, I. Materials in Organic Electrochemical Transistors for Bioelectronic Applications: Past, Present, and Future. *Adv. Funct. Mater*. **2019**, *29*, 1807033.

(3) (a) Su, H.-C.; Chen, Y.-R.; Wong, K.-T. Recent Progress in White Light-Emitting Electrochemical Cells. *Adv. Funct. Mater*. **2020**, *30*, 1906898; (b) Uchida, S.; Nishikitani, Y. Exciplex Emission in Light-Emitting Electrochemical Cells and Light Outcoupling Methods for More Efficient LEC Devices. *Adv. Funct. Mater*. **2020**, *30*, 1907309; (c) Kanagaraj, S.; Puthanveedu, A.; Choe, Y. Small Molecules in Light-Emitting Electrochemical Cells: Promising Light-Emitting Materials. *Adv. Funct. Mater*. **2020**, *30*, 1907126.

(4) (a) Qiao, Q. (Ed.), Iniewski, K. *Organic Solar Cells*, CRC Press, Boca Raton, **2015**; (b) Voronov, M. *Organic Solar Cells: Advances in Research and Applications*, Nova Science Publishers, Inc. **2017**, 119 p.; (c) Tong, Y.; Xiao, Z.; Du, X.; Zuo, C.; Li, Y.; Lv, M.; Yuan, Y.; Yi, C.; Hao, F.; Hua, Y.; Lei, T.; Lin, Q.; Sun, K.; Zhao, D.; Duan, C.; Shao, X.; Li, W.; Yip, H.-L.; Xiao, Z.; Zhang, B.; Bian, Q.; Cheng, Y.; Liu, S.; Cheng, M.; Jin, Z.; Yang, S.; Ding, L. Progress of the key materials for organic solar cells. *Sci. China Chem*. **2020**, *63*, 758-765; (d) Pan, Y.-Q.; Sun, G.-Y. Star-Shaped Non-Fullerene Small Acceptors for Organic Solar Cells. *ChemSusChem* **2019**, *12*, 4570-4600.

(5) (a) Huang, Y.; Hsiang, E.-L.; Deng, M.-Y.; Wu, S.-T. Mini-LED, Micro-LED and OLED displays: present status and future perspectives. *Light: Sci. Appl.* **2020**, *9*, 105; (b) Koden, M. *OLED Displays and Lighting*, John Wiley & Sons, Ltd, UK, **2017**, 209 p.

(6) (a) Pak, Y. L.; Swamy, K. M. K.; Yoon, J. Recent Progress in Fluorescent Imaging Probes. *Sensors* **2015**, *15*, 24374-24396; (b) Suzuki, Y.; Yokoyama, K. Development of Functional Fluorescent Molecular Probes for the Detection of Biological Substances. *Biosensors* **2015**, *5*, 337-363; (c) Park, S.-H.; Kwon, N.; Lee, J.-H.; Yoon, J.; Shin, I. Synthetic ratiometric fluorescent probes for detection of ions. *Chem. Soc. Rev*. **2020**, *49*, 143-179; (d) Chen. Y. Design and construction of COX-2 specific fluorescent probes. *Mol. Cell. Probes* **2019**, *48*, 101472.

(7) (a) Xu, D.; Li, L.; Chu, C.; Zhang, X.; Liu, G. Advances and perspectives in near-infrared fluorescent organic probes for surgical oncology. *WIREs Nanomed Nanobiotechnol*. **2020,** *12*, e1635; (b) Ha, Y.; Choi, H.-K. Recent conjugation strategies of small organic fluorophores and ligands for cancer-specific bioimaging. *Chem. Biol. Interact.* **2016**, *248*, 36-51; (c) Baggaley, E.; Weinstein, J. A.; Williams, J. A. G. Lighting the way to see inside the live cell with luminescent transition metal complexes. *Coord. Chem. Rev*. **2012**, *256*, 1762-1785; (d) Jun, J. V.; Chenoweth, D. M.; Petersson, E. J. Rational design of small molecule fluorescent probes for biological applications. *Org. Biomol. Chem*. **2020**, *18*, 5747-5763.

(8) (a) Birks, J. B. *Photophysics of aromatic molecules*, Wiley- InterScience, London, **1970**, 704 p.; (b) Qi, J.; Hu, X.; Dong, X.; Lu, Y.; Lu, H.; Zhao, W.; Wu, W. Towards more accurate bioimaging of drug nanocarriers: turning aggregation-caused quenching into a useful tool. *Adv. Drug Delivery Rev.* **2019**, *143*, 206-225; (c) Sharma, H.; Kaur, N.; Singh, N. Sensing in aqueous medium: mechanism and its application in the field of molecular recognition. *Anal. Methods*, **2015**, *7*, 7000-7019.

(9) Luo, J.; Xie, Z.; Lam, J. W. Y.; Cheng, L.; Chen, H.; Qiu, C.; Kwok, H. S.; Zhan, X.; Liu, Y.; Zhuc, D.; Tang, B. Z. Aggregation-induced emission of 1-methyl-1,2,3,4,5-pentaphenylsilole. *Chem. Commun*. **2001**, *18*, 1740-1741.

(10) (a) Mei, J.; Leung, N. L. C.; Kwok, R. T. K.; Lam, J. W. Y.; Tang, B. Z. Aggregation-Induced Emission: Together We Shine, United We Soar! *Chem. Rev*. **2015**, *115*, 21, 11718-11940; (b) Yang, J.; Chi, Z.; Zhu, W.; Tang, B. Z.; Li, Z. Aggregation-induced emission: a coming-of-age ceremony at the age of eighteen. *Sci. China Chem.* **2019**, *62*, 1090-1098; (c) Li, X.; Li, M.; Yang, M.; Xiao, H.; Wang, L.; Chen, Z.; Liu, S.; Li, J.; Li, S.; James, T. D. "Irregular" aggregation-induced emission luminogens. *Coord. Chem. Rev.* **2020**, *418*, 213358; (d) Hong, Y.; Lam, J. W. Y.; Tang, B. Z. Aggregation-induced emission. *Chem. Soc. Rev*. **2011**, *40*, 5361-5388.

(11) (a) Grimes, R. N. *Carboranes, 3rd Edition*, Academic Press, New York, **2016**, 1058 p.; (b) Smyshliaeva, L. A.; Varaksin, M. V.; Charushin, V. N.; Chupakhin, O. N. Azaheterocyclic Derivatives of ortho-Carborane: Synthetic Strategies and Application Opportunities. *Synthesis* **2020**, *52*, 337–352.; (c) Núñez, R.; Tarrés, M.; Ferrer-Ugalde, A.; de Biani, F. F.; Teixidor, F. Electrochemistry and Photoluminescence of Icosahedral Carboranes, Boranes, Metallacarboranes, and Their Derivatives. *Chem. Rev.* **2016**, *116*, 14307–14378; (d) Sivaev, I.; Bregadze, V. 1,1'-Bis(*ortho*-carborane)-based transition metal complexes. *Coord. Chem. Rev*. **2019**, *392*, 146–176; (e) Quan, Y.; Xie, Z. Controlled functionalization of o-carborane via transition metal catalyzed B–H activation. *Chem. Soc. Rev*. **2019**, *48*, 3660-3673; (f) Eleazer, B. J.; Peryshkov, D.V. Coordination

Chemistry of Carborane Clusters: Metal-Boron Bonds in Carborane, Carboranyl, and Carboryne Complexes. *Comments Inorg. Chem.*, **2018**, *38*, 79-109.

(12) (a) Ochi, J.; Tanaka, K.; Chujo, Y. Recent Progress in the Development of Solid-State Luminescent o-Carboranes with Stimuli Responsivity. *Angew. Chem. Int. Ed.* **2020**, *59*, 9841-9855; (b) Núñez, R.; Romero, I.; Teixidor, F.; Viñas, C. Icosahedral boron clusters: a perfect tool for the enhancement of polymer features. *Chem. Soc. Rev*. **2016**, *45*, 5147-5173.

(13) (a) Zhu, Y.; Hosmane, N. S. Advanced carboraneous materials. *J. Organomet. Chem*. **2017**, *849-850*, 286-292; (b) Jeans, R. J.; Chan, A. P. Y.; Riley, L. E.; Taylor, J.; Rosair, G. M.; Welch, A. J.; Sivaev, I.B. Arene–Ruthenium Complexes of 1,1′-Bis(ortho-carborane): Synthesis, Characterization, and Catalysis. *Inorg. Chem.* **2019**, *58*, 11751-11761; (c) Hosmane, N. S. in *Handbook of Boron Science With Applications in Organometallics, Catalysis, Materials and Medicine (In 4 Volumes*), (Eds.: Hosmane, N. S.; Eagling, R.), World Scientific, **2018**, 1056 p.; (d) Fisher, S. P.; Tomich, A. W.; Lovera, S. O.; Kleinsasser, J. F.; Guo, J.; Asay, M. J.; Nelson, H. M.; Lavallo, V. Nonclassical Applications of closo-Carborane Anions: From Main Group Chemistry and Catalysis to Energy Storage. *Chem. Rev.* **2019**, *119*, 8262–8290; (e) Vinogradov, M. M.; Loginov, D. A. Rhoda- and iridacarborane halide complexes: Synthesis, structure and application in homogeneous catalysis. *J. Organomet. Chem*. **2020**, *910*, 121135; (f) Yinghuai, Z.; Hosmane, N. S. Carborane-based transition metal complexes and their catalytic applications for olefin polymerization: Current and future perspectives. *J. Organomet. Chem*. **2013**, *747*, 25-29.

(14) (a) Stockmann, P.; Gozzi, M.; Kuhnert, R.; Sarosi, M. B.; Hey-Hawkins, E. New keys for old locks: carborane-containing drugs as platforms for mechanism-based therapies. *Chem. Soc. Rev.* **2019**, *48*, 3497-3512; (b) Ali, F.; Hosmane, N. S.; Zhu, Y. Boron Chemistry for Medical Applications. *Molecules* **2020**, *25*, 828; (c) Calabrese, G.; Daou, A.; Barbu, E.; Tsibouklis, J. Towards carborane-functionalised structures for the treatment of brain cancer. *Drug Discovery Today* **2018**, *23*, 63-75; (d) Scholz, M. S.; Wingen, L. M.; Brunst, S.; Wittmann, S. K.; Cardoso, I. L. A.; Weizel,

L.; Proschak, E. Soluble epoxide hydrolase inhibitors with carboranes as non-natural 3-D pharmacophores. *Eur. J. Med. Chem.* **2020**, *185*, 111766; (e) Agarwal, H. K.; Hasabelnaby, S.; Tiwari, R.; Tjarks, W. Boron Cluster (Radio) Halogenation in Biomedical Research. In *Boron Science: New Technologies and Applications1st Edition*; Hosmane, N. S., Ed.; CRC Press: BocaRaton, FL, 2012; pp 107-146; (f) Viñas, C.; Núñez, R.; Bennour, I.; Teixidor, F. Periphery Decorated and Core Initiated Neutral and Polyanionic Borane Large Molecules: Forthcoming and Promising Properties for Medicinal Applications. *Curr. Med. Chem*. **2019**, *26*, 5036-5076; (g) Alamón, C.; Dávila, B.; García, M.F.; Sánchez, C.; Kovacs, M.; Trias, E.; Barbeito, L.; Gabay, M.; Zeineh, N.; Gavish, M.; Teixidor, F.; Viñas, C.; Couto, M.; Cerecetto, H. Sunitinib-Containing Carborane Pharmacophore with the Ability to Inhibit Tyrosine Kinases Receptors FLT3, KIT and PDGFR-β, Exhibits Powerful In Vivo Anti-Glioblastoma Activity. *Cancers* **2020**, *12*, 3423.

(15) (a) Dong, B.; Oyelade, A.; Kelber, J. A. Carborane-based polymers: a novel class of semiconductors with tunable properties. *Phys. Chem. Chem. Phys*. **2017**, *19*, 10986-10997; (b) Şener, S. Ball-Type Dioxy-o-Carborane Bridged Cobaltphthalocyanine: Synthesis, Characterization and DFT Studies For Dye-Sensitized Solar Cells as Photosensitizer. *Heterocycl. Commun*. **2020**, *26*, 1, 37-45; (c) Kim, B. G.; Jang, W.; Jeon, H.; Lee, S.; Han, W.-S.; Wang, D. H. An unusual charge transfer accelerator of monomolecular Cb-OMe (4,4'-(ortho-carborane)bis(N,N-bis(4-methoxyphenyl)aniline) in perovskite optoelectronic devices. *Sol. Energy Mater. Sol. Cells* **2020**, *208*, 110414; (d) Chang, Z.; Okoye, N. C.; Urffer, M. J.; Miller, L. F. Enhancement Effect of Fused Double Benzene-Ring Structure on the Light Output of Carborane-Loaded Toluene- and Pseudocumene-Based Scintillators. *IEEE Trans. Nucl. Sci.* **2016**, *63*, 3, 1750-1761; (e) Chang, Z.; Okoye, N. C.; Urffer, M. J.; Green, A. D.; Childs, K. E.; Miller. L. F. On the scintillation efficiency of carborane-loaded liquid scintillators for thermal neutron detection. *Nucl. Instrum. Methods Phys. Res., Sect. A.* **2015**, *769*, 112-122.

(16) (a) Wua, X.; Guo, J.; Jia. W.; Zhao, J.; Jia, D.; Shan, H. Highly-efficient solid-state emission of tethered anthracene-o-carborane dyads and their visco- and thermo-chromic luminescence properties. *Dyes Pigm.* **2019**, *162*, 855-862; (b) Wu, X.; Guo, J.; Zhao, J.; Che, Y.; Jia, D.; Chen, Y. Multifunctional luminescent molecules of o-carborane-pyrene dyad/triad: flexible synthesis and study of the photophysical properties. *Dyes Pigm*. **2018**, *154*, 44-51; (c) Chaari, M.; Cabrera-González, J.; Kelemen, Z.; Viñas, C.; Ferrer-Ugalde, A.; Choquesillo-Lazarte, D.; Salah, A. B.; Teixidor, F.; Núñez, R. Luminescence properties of carborane-containing distyrylaromatic systems. *J. Organomet. Chem*. **2018**, *865*, 206-213; (d) Mukherjee, S.; Thilagar, P. Boron clusters in luminescent materials. *Chem. Commun*. **2016**, *52*, 1070-1093; (e) Ferrer-Ugalde, A.; González-Campo, A.; Viñas, C.; Rodríguez-Romero, J.; Santillan, R.; Farfán, N.; Sillanpää, R.; Sousa-Pedrares, A.; Núñez, R.; Teixidor, F. Fluorescence of New o-Carborane Compounds with Different Fluorophores: Can it be Tuned? *Chem. Eur. J.* **2014**, *20*, 9940-9951; (f) Ferrer-Ugalde, A.; Cabrera-González, J.; Juárez-Pérez, E. J.; Teixidor, F.; Pérez-Inestrosa, E.; Montenegro, J. M.; Sillanpää, R.; Haukka, M.; Núñez, R. Carborane–stilbene dyads: the influence of substituents and cluster isomers on photoluminescence properties. *Dalton Trans*. **2017**, *46*, 2091-2104.

(17) (a) Wu, X.; Guo, J.; Lv, Y.; Jia, D.; Zhao, J.; Shan, H.; Jin, X.; Ma, Y. Aggregation-induced emission characteristics of o-carborane-functionalized fluorene and its heteroanalogs: the influence of heteroatoms on photoluminescence. *Mater. Chem. Front*. **2020**, *4*, 257-267; (b) Böhling, L.; Brockhinke, A.; Kahlert, J.; Weber, L.; Harder, R.A.; Yufit, D. S.; Howard; J. A. K.; MacBride, J. A. H.; Fox, M. A. Substituent Effects on the Fluorescence Properties of ortho-Carboranes: Unusual Emission Behaviour in C-(2′-Pyridyl)-orthocarboranes. *Eur. J. Inorg. Chem.* **2016**, 403-412.

(18) (a) Nakazato, T.; Kamatsuka, T.; Inoue, J.; Sakurai, T.; Seki, S.; Shinokubo, H.; Miyake, Y. The reductive aromatization of naphthalene diimide: a versatile platform for 2,7-diazapyrenes. *Chem. Commun.* **2018**, *54*, 5177-5180; (b) Zhou, K.; Dong, H.; Zhang, H.; Hu, W. High performance n-type and ambipolar small organic semiconductors for organic thin film transistors.

Phys. Chem. Chem. Phys. **2014**, *16*, 22448-22457; (c) Zhao, X.; Zhan, X. Electron transporting semiconducting polymers in organic electronics. *Chem. Soc. Rev*. **2011**, *40*, 3728-3743; (d) Usta, H.; Facchetti, A.; Marks, T. J. n-Channel Semiconductor Materials Design for Organic Complementary Circuits. *Acc. Chem. Res.* **2011**, *44*, 7, 501–510; (e) Shi, Y.-R.; Wei, H.-L.; Liu, Y.-F. The role of electron-attracting substituents and molecular stacking motifs in the charge transport of tetraazapyrene derivatives. *New J. Chem*. **2019**, *43*, 5706-5718.

(19) Geib, S.; Martens, S. C.; Zschieschang, U.; Lombeck, F.; Wadepohl, H.; Klauk, H.; Gade, L. H. 1,3,6,8-Tetraazapyrenes: Synthesis, Solid-State Structures, and Properties as Redox-Active Materials. *J. Org. Chem*. **2012**, *77*, 14, 6107-6116.

(20) Sun, J.; Liu, Z.; Liu, W.-G.; Wu, Y.; Wang, Y.; Barnes, J. C.; Hermann, K. R.; Goddard, W. A.; Wasielewski, M. R.; Stoddart, J. F. Mechanical-Bond-Protected, Air-Stable Radicals. *J. Am. Chem. Soc.* **2017**, *139*, 36, 12704-12709.

(21) (a) Becker, H.-C.; Nordén, B. DNA Binding Properties of 2,7-Diazapyrene and Its N-Methylated Cations Studied by Linear and Circular Dichroism Spectroscopy and Calorimetry. *J. Am. Chem. Soc*. **1997**, *119*, 25, 5798-5803; (b) Piantanida, I.; Tomišić, V.; Žinić, M. 4,9-Diazapyrenium cations. Synthesis, physico-chemical properties and binding of nucleotides in water. *J. Chem. Soc., Perkin Trans*. **2000**, *2*, 375-383.

(22) (a) Steiner-Biocić, I.; Glavas-Obrovac, L.; Karner, I.; Piantanida, I.; Zinić, M.; Pavelić, K.; Pavelić, J. 4,9-Diazapyrenium Dications Induce Apoptosis in Human Tumor Cells. *Anticancer Res.* **1996**, *16* (6B), 3705–3708; (b) Roknić, S.; Glavaš-Obrovac, L.; Karner, I.; Piantanida, I.; Žinić, M.; Pavelić, K. In vitro Cytotoxicity of Three 4,9-Diazapyrenium Hydrogensulfate Derivatives on Different Human Tumor Cell Lines. *Chemotherapy* **2000**, *46*, 2, 143-149.

(23) (a) Omura, Y.; Tachi, Y.; Okada, K.; Kozaki, M. Synthesis and Properties of Nitrogen-Containing Pyrenes. *J. Org. Chem.* **2019**, *84*, 4, 2032-2038; (b) Verbitskiy, E. V.; Dinastiya, E. M.; Eltsov, O. S.; Zhilina, E. F.; Schepochkin, A. V.; Rusinov, G. L.; Chupakhin, O. N.; Charushin, V. N.

Assembly of annulated 1,3-diazapyrenes by consecutive cross-coupling and cyclodehydrogenation of (het)arene moieties. *Mendeleev Commun*. **2020**, *30*, 2, 142-144; (c) Jayakumar, J.; Cheng, C.-H. Recent Advances in the Synthesis of Quaternary Ammonium Salts via Transition-Metal-Catalyzed C-H Bond Activation. *J. Chin. Chem. Soc*. **2018**, *65*, 11-23.

(24) (a) Aksenov, A. V.; Borovlev, I. V.; Aksenova, I. V.; Pisarenko, S. V.; Kovalev, D. A. A new method for [c,d]pyridine peri-annelation: synthesis of azapyrenes from phenalenes and their dihydro derivatives. *Tetrahedron Lett.* **2008**, *49*, 4, 707-709; (b) Aksenov, A. V.; Borovlev, I. V.; Aksenova, I. V.; Lyakhovnenko, A. S.; Kovalev, D. A. Synthesis of 1,3,7-triazapyrene and 1,2,3,7-tetraazapyrene derivatives as a result of anomalous Hoesch reaction. *Russ Chem Bull*. **2008**, *57*, 217-218; (c) Aksenov, A. V.; Aksenov, N. A.; Lyakhovnenko, A. S.; Kumshaeva, A. B.; Aksenova, I. V. Novel three-component reaction of perimidines with 1,3,5-triazines and carbonyl compounds in polyphosphoric acid. an efficient method for peri-annelation of a carbocyclic and pyridine ring. *Chem. Heterocycl. Comp*. **2012**, *48*, 634-641; (d) Aksenova, I. V.; Aksenov, A. V.; Lyakhovnenko, A. S.; Borovlev, I. V. Unexpected reaction of 1,8-naphthylenediamine and perimidines with 1,3,5-triazine in the presence of benzonitrile in polyphosphoric acid. *Chem. Heterocycl. Comp*. **2008**, *44*, 891-892; (e) Aksenov, A. V.; Lyahovnenko, A. S.; Aksenova, I. V.; Nadein, O. N. New tri-component peri-annelation reactions of carbocyclic and pyridine ring to perimidines – the synthesis of 1,3-diazapyrenes and 1,3,7-triazapyrenes. *Tetrahedron Lett*. **2008**, *49*, 1808-1811.

(25) Borovlev, I. V.; Demidov, O. P.; Saigakova, N. A. SNH Arylation of 1,3,7-triazapyrenes in acidic aqueous solution. *Chem. Heterocycl. Comp.* **2013***, 49*, 618–623.

(26) Demidov, O. P.; Borovlev, I. V.; Saigakova, N. A.; Nemykina, O. A.; Pisarenko, S. V. Synthesis and cleavage of 1,3,7-triazapyrene ethers. *Chem. Heterocycl. Comp*. **2013**, *48*, 1527-1532.

(27) (a) Borovlev, I.; Demidov, O.; Saigakova, N.; Pisarenko, S.; Nemykina, O. An oxidative alkylamination of 1,3,7-triazapyrenes in the aqueous medium. *J. Heterocyclic Chem*. **2011**, *48*, 1206-1210; (b) Borovlev, I. V.; Demidov, O. P.; Saigakova, N. A. Arylamination of 1,3,7-

Triazapyrene. *Chem. Heterocycl. Comp*. **2014**, *50*, 685-690; (c) Borovlev, I. V.; Demidov, O. P.; Kurnosova, N. A.; Avakyan, E. K.; Amangazieva, G. A. Synthesis of heterofunctional 1,3,7-triazapyrene derivatives by SNH and SNAr reactions. *Russ. J. Org. Chem*. **2015**, *51*, 1438-1443.

(28) (a) Borovlev, I.; Demidov, O.; Saigakova, N.; Amangasieva, G. SNH- and SNipso-Arylamination of 1,3,7-Triazapyrenes. *Eur. J. Org. Chem*. **2014**, *34*, 7675-7683; (b) Amangasieva, G. A.; Borovlev, I. V.; Demidov, O. P.; Kurnosova, N. A.; Avakyan, E. K. Urea in an aminodemethoxylation reaction of 6-methoxy-1,3,7-triazapyrenes. *Chem. Heterocycl. Compd*. **2015**, *51*, 586-588; (c) Borovlev, I. V.; Demidov, O. P.; Amangasieva, G. A.; Avakyan, E. K.; Kurnosova, N. A. Ureas as new nucleophilic reagents for SNH amination and carbamoyl amination reactions in the 1,3,7-triazapyrene series. *Arkivoc* **2016**, *iii*, 58-70; (d) Borovlev, I.; Demidov, O.; Amangasieva, G.; Avakyan, E.; Kurnosova, N. Ureas as a New Nucleophilic Reagents for SNAr Amination and Carbamoyl Amination Reactions in 1,3,7-Triazapyrene Series. *J. Heterocyclic Chem.* **2017**, *54*, 406-412.

(29) (a) Charushin, V. N.; Chupakhin, O. N. Nucleophilic C—H functionalization of arenes: a contribution to green chemistry. *Russ. Chem. Bull*. **2019**, *68*, 453-471; (b) Dyker, G. *Handbook of C-H Transformations: Applications in Organic Synthesis*, Wiley-VCN, Weinheim, **2005**; (c) Murakami, K.; Yamada, S.; Kaneda, T.; Itami, K. C–H Functionalization of Azines. *Chem. Rev.* **2017**, *117*, 9302-9332; (d) Ghosh, P.; Ganguly, B.; Das, S. C–H functionalization of quinazolinones by transition metal catalysis. *Org. Biomol. Chem*. **2020**, *18*, 4497-4518; (e) Latha, D. S.; Yaragorla, S. C(sp3)-H Functionalization of 2-Methyl Azaarenes: Highly Facile Approach to Aza-Heterocyclic Compounds. *Eur. J. Org. Chem.* **2020**, *15*, 2155-2179; (f) Morimoto, K.; Dohi, T.; Kita, Y. Metal-free Oxidative Cross-Coupling Reaction of Aromatic Compounds Containing Heteroatoms. *Synlett* **2017**, *28*, 1680-1694.

(30) (a) Chupakhin, O. N.; Charushin, V. N. Nucleophilic C-H functionalization of arenes: A new logic of organic synthesis Expanding the scope of nucleophilic substitution of hydrogen in

aromatics. *Pure Appl. Chem*. **2017**, *89*, 1195-1208; (b) Chupakhin, O. N.; Charushin, V. N. Recent advances in the field of nucleophilic aromatic substitution of hydrogen. *Tetrahedron Lett*. **2016**, *57*, 2665-2672; (c) Charushin, V. N.; Chupakhin, O. N. (Eds.), Metal-Free C–H Functionalization of Aromatics: Nucleophilic Displacement of Hydrogen. In Series: *Top. Heterocycl. Chem*., vol. 37, Springer, Heidelberg, **2014**, 283 p; (d) Mąkosza, M. Nucleophilic substitution in nitroarenes: a general corrected mechanism. *ChemTexts* **2019**, *5*, 10.

(31) Popescu, A.-R.; Musteti, A. D.; Ferrer-Ugalde, A.; Viñas, C.; Núñez, R.; Teixidor, F. Influential Role of Ethereal Solvent on Organolithium Compounds: The Case of Carboranyllithium. *Chem. – Eur. J.* **2012**, *18*, 3174-3184.

(32) Akulov, A. A.; Varaksin, M. V.; Mampuys, P.; Charushin, V. N.; Chupakhin, O. N.; Maes, B. U. W. C(sp2)–H functionalization in non-aromatic azomethine-based heterocycles. *Org. Biomol. Chem*. **2021**,*19*, 297-312.

(33) Islam, Md. M.; Hu, Z.; Wang, Q.; Redshaw, C.; Feng, X. Pyrene-based aggregation-induced emission luminogens and their applications. *Mater. Chem. Front*. **2019**, *3*, 762-781.

(34) Kim, S.; Lee, J. H.; So, H.; Kim, M.; Mun, M. S.; Hwang, H.; Park, M. H.; Lee, K. M. Insights into the effects of substitution position on the photophysics of mono-o-carborane-substituted pyrenes. *Inorg. Chem. Front.* **2020**, *7*, 2949-2959.

(35) (a) Chen, Y.; Guo, J.; Wu, X.; Jia, D.; Tong, F. Color-tuning aggregation-induced emission of o-Carborane-bis(1,3,5-triaryl-2-pyrazoline) triads: Preparation and investigation of the photophysics. *Dyes Pigm.* **2018**, *148*, 180-188; (b) Naito, H.; Nishino, K.; Morisaki, Y.; Tanaka, K.; Chujo, Y. Luminescence Color Tuning from Blue to Near Infrared of Stable Luminescent Solid Materials Based on Bis-o-Carborane-Substituted Oligoacenes. *Chem. Asian J.* **2017**, *12*, 2134-2138; (c) Shin, N.; Yu, S.; Lee, J. H.; Hwang, H.; Lee, K. M. Biphenyl- and Fluorene-Based o-Carboranyl Compounds: Alteration of Photophysical Properties by Distortion of Biphenyl Rings. *Organometallics* **2017**, *36*, 1522-1529; (d) Kwon, S.; Wee, K.-R.; Cho, Y.-J.; Kang, S.O. Carborane

Dyads for Photoinduced Electron Transfer: Photophysical Studies on Carbazole and Phenyl-o -carborane Molecular Assemblies. *Chem. Eur. J.* **2014**, *20*, 5953-5960; (e) Li, X.-Q.; Wang, C.-H.; Zhang, M.-Y.; Zou, H.-Y.; Ma, N.-N.; Qiu, Y.-Q. Tuning second-order nonlinear optical properties of the two-dimensional benzene/carborane compounds with phenyl carbazoles: Substituent effect and redox switch. *J. Organomet. Chem.* **2014**, *749*, 327-334.

(36) D. Jacquemin, V. Wathelet, E. A. Perpète and C. Adamo. Extensive TD-DFT Benchmark: Singlet-Excited States of Organic Molecules. *J. Chem. Theory Comput.*, 2009, **5**, 2420–2435.

(37) N. M. O'boyle, A. L. Tenderholt and K. M. Langner. cclib: A library for package-independent computational chemistry algorithms. *J. Comput. Chem.*, 2008, **29**, 839–845.

(38) Wu, X.; Guo, J.; Quan, Y.; Jia, W.; Jia, D.; Chen, Y.; Xie, Z. Cage carbon-substitute does matter for aggregation-induced emission features of o-carborane-functionalized anthracene triads. *J. Mater. Chem. C* **2018**, *6*, 4140-4149.

(39) Abd-El-Aziz, A. S.; Abdelghani, A. A.; Wagner, B. D.; Abdelrehim, E. M. Aggregation enhanced excimer emission (AEEE) with efficient blue emission based on pyrene dendrimers. *Polym. Chem*. **2016**, *7*, 3277-3299.

(40) (a) Rostami, Z.; Hosseinian, A.; Monfared, A. DFT results against experimental data for electronic properties of C 60 and C 70 fullerene derivatives. *J. Mol. Graph. Model*. **2018**, *81*, 60-67; (b) Zhang, G.; Musgrave, C. B. Comparison of DFT Methods for Molecular Orbital Eigenvalue Calculations. *J. Phys. Chem. A* **2007**, *111*, 1554-1561.

(41) Molenda, R.; Boldt, S.; Villinger, A.; Ehlers, P.; Langer, P. Synthesis of 2-Azapyrenes and Their Photophysical and Electrochemical Properties. *J. Org. Chem.* **2020**, *85*, 12823-12842.